Inorganic Chemistry

Article

pubs.acs.org/IC

A Study on Zr−Ir Multiple Bonding Active for C−H Bond Cleavage

Masataka Oishi,[†] Masato Oshima,[‡] and Hiroharu Suzuki*,[†]

[†]Graduate School of Science and Engineering, Tokyo Institute of Technology, 2-12-1 O-okayama, Meguro-ku, Tokyo 152-8552, Japan

[‡]School of Engineering, Tokyo Polytechnic University, 1583 Iiyama, Atsugi-shi, Kanagawa 243-0297, Japan

Supporting Information

ABSTRACT: Zr−Ir hydrido complexes with *ansa*-(cyclopentadienyl)-(amide) as the supporting ligand in the zirconium fragment, e.g., $(L^1ZrR)(Cp^*Ir)(\mu\text{-}H)_3$ [$L^1 = Me_2Si(\eta^5\text{-}C_5Me_4)(N^tBu)$, R = Cl (**5**), Ph (**7**), Me (**10**), alkyl, and aryl] were designed, synthesized, and isolated as tractable early−late heterodinuclear complexes. Despite the presence of the three supporting hydride ligands, Zr−Ir distances in the crystal structures of **5**, alkyl, and aryl complexes [2.74−2.76 Å] were slightly longer than the sum of the element radii of Zr and Ir [2.719 Å]. These hydrocarbyl complexes displayed the thermolytic C−H activation of a variety of aromatic compounds and several organometallic compounds. Also, the substrate scope and limitation in the Zr−Ir system were studied. The regiochemical outcomes during the C−H activation of pyridine derivatives and methoxyarenes suggested the *in situ* generation of a Lewis acidic active intermediate, i.e., $(L^1Zr)(Cp^*IrH_2)$ (**III**). The existence of **III** and relevant σ-complex intermediates $\{L^1Zr(\eta^2\text{-}R{-}H)\}(Cp^*IrH_2)$ ($\mathbf{II_R}$) (R = Me, Ph) in the ligand exchange was demonstrated by the direct isolation of a Et_3PO-adduct of **III** (**39b**) from **7** and kinetic studies. The structure of the direct Zr−Ir bonds in $\mathbf{II_{Ph}}$, $\mathbf{II_{Me}}$, **III**, and **39b** were probed using computational studies. The unprecedented strong M−M′ interactions in the early−late heterobimetallic (ELHB) complexes have been proposed herein.

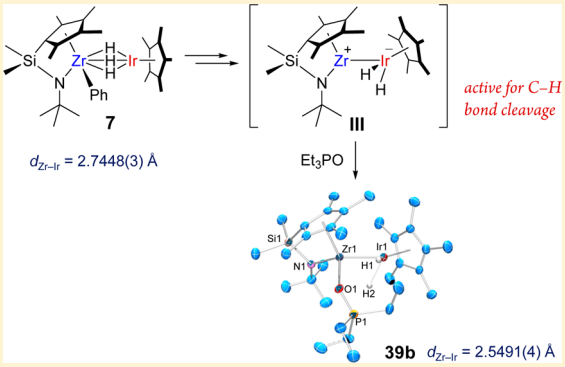

INTRODUCTION

Direct interactions between early and late transition-metal centers have received considerable attention since the discovery of the promotion effects in the area of surfaced catalysis, e.g., the Fischer−Tropsch process.[1] One of the promotion phenomena, classically called "strong metal−support interactions" (SMSI),[2] undoubtedly emphasizes a potential of superior roles of early metal-oxide support toward late metal-catalyst centers, in which formation of a direct $M_{early}{-}M_{late}$ bond have been deduced to provide dramatic change in catalyst activity and selectivity. In order to invent homogeneous CO hydrogenation systems relevant to the above heterogeneous catalysis, Casey and co-workers have commenced pioneering works using homogeneous transition-metal chemistry, in particular, the synthesis of close and disparate $M_{early}{-}M_{late}$ bonded binuclear carbonyl complexes with a heterodifunctional ligand and oxocarbene formation (Scheme 1).[3]

While a number of early late heterobimetallic (ELHB) complexes have been synthesized to date, the reaction chemistry of the direct $M_{early}{-}M_{late}$ bonds still remains limited.[4] We reason that decomposition of the $M_{early}{-}M_{late}$ single bonds may readily occur once employed for oxidative addition of reagents.[5] Gade and co-workers have developed various new stoichiometric reactions exploiting the advantage of the reactive unsupported $M_{early}{-}M_{late}$ bonds.[6] Among many examples several group 4−group 9 metal bonded complexes represented in Chart 1 have been successfully studied on cooperative reactivity. Bergman and Erker introduced bridged zirconocene-based Zr−Ir and Zr−Rh ELHB complexes with a direct metal−metal bond (A and B in Chart 1). They reported cooperative reactivities in stoichiometric and catalytic reactions.[7,8] Multiply supported Zr−Rh and Zr−Co complexes with direct σ-bonds and dative bonds were described by Wolczanski and Thomas (C and D in Chart 1), whose groups studied the durable $M_{early}{-}M_{late}$ bonds for small molecule activations.[9,10] Use of multiple bridges in the $M_{early}{-}M_{late}$ bonded systems is apparently an excellent approach to protect them from decomposition, but they sacrifice reactivity to some extent.

In our research program, reversible formation of unsupported multiple bonds between early and late transition metals is the focus. Their reactivity can be expected to be higher than that for $M_{early}{-}M_{late}$ σ-bonds because π- or δ-based bonding usually lie higher in energy than the corresponding σ-bond. We have recently disclosed oxidative addition chemistry of Ta−Ir double bonds.[11] Unlike the previous examples, with the unsupported $M_{early}{-}M_{late}$ single bond,[5,6] $\{Cp^*Ta(CH_2SiMe_3)_2\}(Cp^*IrH_2)$, designed to have labile hydride ligands and Cp* as a facial supporting ligand, enables oxidative addition of C−H, N−H, and O−H bonds to the Ta−Ir double bond without extensive complex decomposition (Scheme 2).

Received: February 1, 2014
Published: June 10, 2014

Scheme 1. Oxidative Addition of H_2 and Carbene Formation on M_{early}–M_{late} Bonded Carbonyls

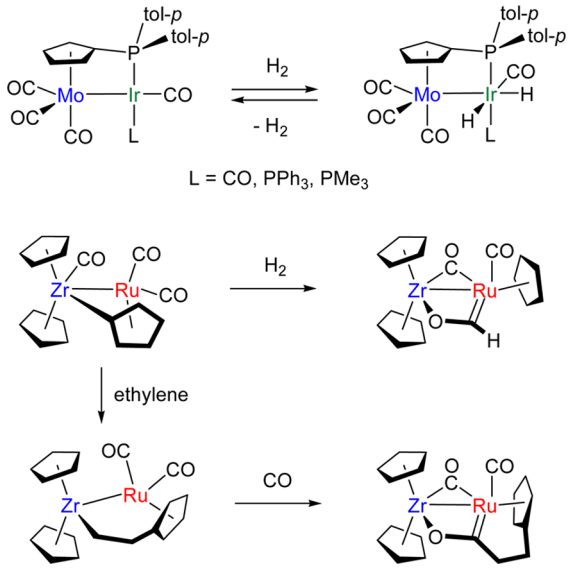

As outlined in Scheme 3, we have also preliminarily showed that zirconocene–Ir hydrides **3**, derived from chlorido complexes **1**, displays reversible arene C–H activation and ultimate dimerization to stable planar-square Zr_2Ir_2 hydrido complex **4**.[12] Stoichiometric intermolecular C–H activation of a variety of alkanes and nonactivated aromatic compounds using neutral mononuclear Group 4 or Group 9 metal complexes has been developed.[13−15] In our system, we propose that the reaction proceeds through a Zr–Ir directly bonded species **2**. Irreversible formation of **4** has hampered attempts to gain a better understanding of the proposed transient species **2**. Therefore, we turned our attention to modify the early metal supporting ligand, so that, in this study, the bis(cyclopentadienyl) ligand system was replaced by *ansa*-mono(cyclopentadienyl)amides. Here, we report the bimetallic C–H activation chemistry and evidence of the formation of the Zr–Ir direct bond.

■ RESULTS AND DISCUSSION

I. Design, Synthesis, and Structure of Zr–Ir Complexes. *1. Design and Synthesis.* First of all, two *ansa*-(cyclopentadienyl)amide ligands were used in this study: one is commercially available, $Me_2Si(C_5Me_4)(NBu^t)^{2-}$ (L^1) and the other is a nonmethylated analogue of L^1, $Me_2Si(C_5H_4)(NBu^t)^{2-}$ (L^2). According to literature procedures,[16] the corresponding zirconium dichlorides were prepared from $Zr(NMe_2)_4$ via amine elimination with L^1H_2 and L^2H_2, followed by NMe_2/Cl exchange with Me_3SiCl. In turn, reaction of the zirconium dichlorides with $Li[Cp^*IrH_3]$ afforded $(L^1ZrCl)(Cp^*Ir)(\mu\text{-}H)_3$ (**5**) and $(L^2ZrCl)(Cp^*Ir)(\mu\text{-}H)_3$ (**6**) with good to excellent yields (see Scheme 4). **5** and **6** were treated next with equimolar amounts of PhLi in C_6D_6 or toluene, and phenyl complexes **7** and **8** were formed. This is in preference to nucleophilic abstraction of the bridging hydride ligands that were observed in the reaction of **1** with organolithium reagents.[12]

Complex **7** is stable at ambient temperature in a glovebox for more than a year, whereas **8** loses benzene in C_6D_{12} solution slowly at 25 °C or more quickly at 90 °C (1 h), leading to the formation of dimeric *syn*- and *anti*-hydrides $(L^2Zr)_2(Cp^*Ir)_2(\mu_3\text{-}H)_4$ (**9**). The structures of stereoisomeric **9** were determined by NMR and single-crystal XRD analysis of eventually separated crystals of the two isomers from cyclohexane (Figure 1). Selected bond distances and angles of **9** are listed in Table 1. The mean Zr–Ir distances of **9** (2.73 Å) and nearly planar tetrametallic backbone are comparable with those for the previously reported **4**. Unlike the solution structures of **4** having C_{2v}-symmetric zirconocene units and *anti*-**9**, in the ^1H NMR spectrum of *syn*-**9** (in C_6D_6 at 25 °C), two broad resonances for the four hydride ligands were observed at δ −8.26 and −15.87 ppm in a 1:1 integration ratio, which should be two sets of two equivalent hydrides on each plane of the Zr_2Ir_2 square. To our knowledge, this type of planar square Zr_2Ir_2 tetrahydrides (e.g., **4** and **9**) is likely to be thermally quite stable and does not undergo reversible dissociation to the corresponding binuclear species, even in the presence of dihydrogen or aromatic compounds. Switching L^2 to a sterically more demanding L^1 in the early metal fragment could successfully prevent undesired formation of a Zr_2Ir_2 analogue of **9**, and allowed us to investigate the binuclear structures and their reactivities in this work.

As summarized in Scheme 5, we examined the synthesis of **10**–**17** from **5** with organolithium reagents to evaluate the generality of the organolithium synthetic method. Initial attempts to use MeLi toward **5** in ether solvent resulted in disruption of the bimetallic structure and isolation of mononuclear L^1ZrMe_2. However, the yield of **10** was greatly enhanced when toluene was used as a solvent (97% yield). Similarly, treatment of **5** with other ether-free hydrocarbon-soluble BuLi and Me_3SiCH_2Li gave **11** and **12** quantitatively. Complex **11**, however, slowly decomposed in C_6D_{12} with evolution of *n*-butane (^1H NMR assay). In C_6D_6 solvent, **11** underwent ligand exchange at 25 °C to produce thermally more stable **7**-d_6. Aryllithium reagents can be employed more successfully to isolate arylation products **13**–**17**. Bulky 2,6-dimethoxyphenyllithium, prepared regioselectively from dimethylresorcinol and BuLi, was reluctant to undergo arylation,

Chart 1. Directly Zr–Group 9 Metal-Bonded ELHB Complexes with Bridging Ligands

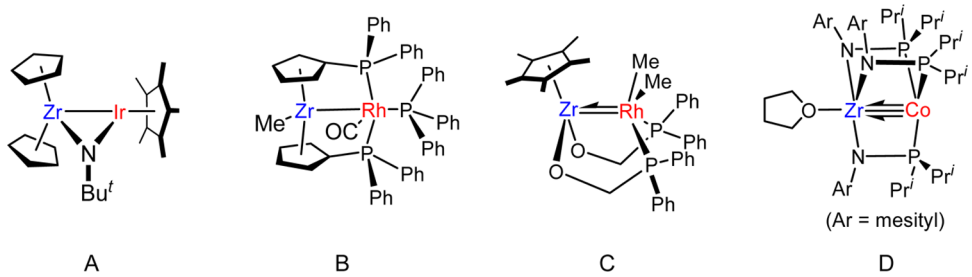

dx.doi.org/10.1021/ic500258g | Inorg. Chem. 2014, 53, 6634–6654

Scheme 2. Oxidative Addition of Ammonia N−H and Phenol O−H Bonds to Ta−Ir Complex

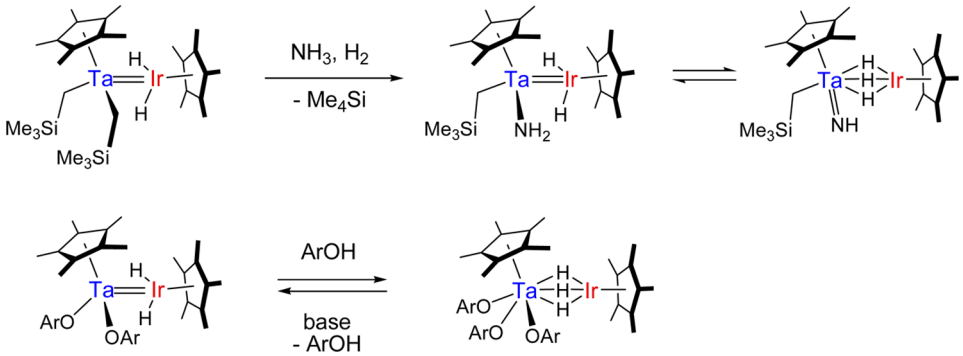

Scheme 3. Ligand Elimination of Zirconocene−Ir Hydrides

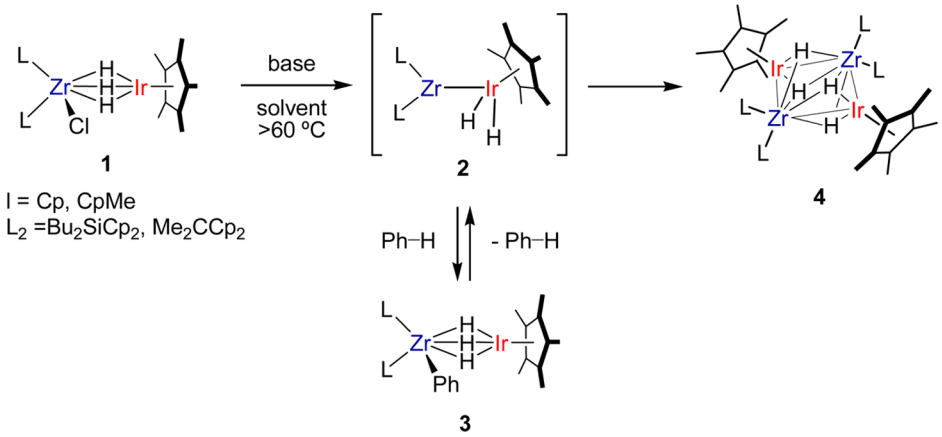

Scheme 4. Synthesis and Stability of Complexes 7 and 8

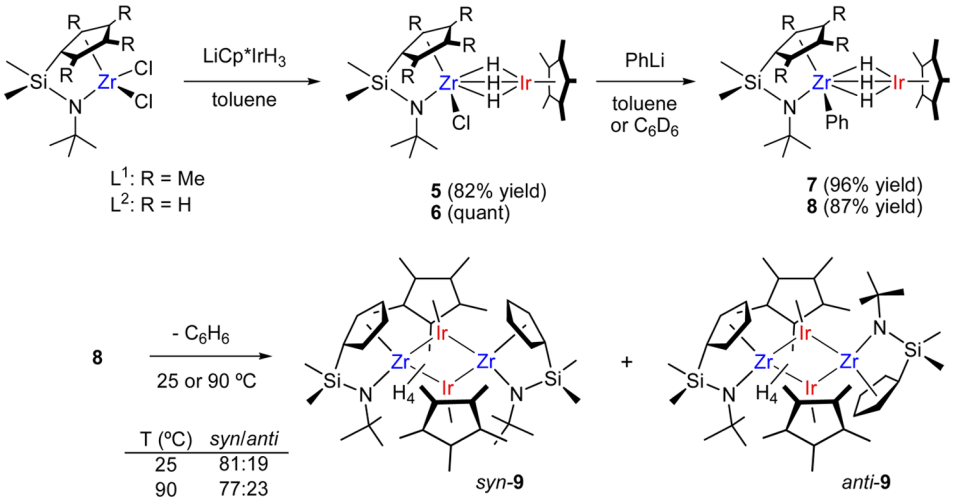

even at elevated temperature for steric reasons. 2-Furyllithium is thermally stable but hardly soluble in toluene. Unlike the formation of **16**, in the reaction between **5** and 2-furyllithium reagent, the addition of a small amount of THF was efficacious, giving rise to the desirable 2-furyl derivative **17**.

*2. Structure of (L[1]ZrR)(Cp*Ir)(μ-H)$_3$.* The above hydrocarbyl Zr−Ir complexes obtained from **5** and organolithiums are air- and moisture-sensitive, and some of them could be isolated as single crystals by recrystallization. Crystal structures of **5** and **13b** are shown in Figure 2, and selected bond distances and angles of crystallographically characterized **5**, **7**, **12**, **13b**, and **17** are listed in Table 2. Each structure has a Zr−Ir distance of 2.739−2.778 Å, the formal shortness ratio (FSR) being 1.01−1.02.[17] These Zr−Ir distances would result from three-center two-electron (3c−2e) interactions among the Zr, Ir, and H atoms. However, from literature criteria,[4c] the FSR does not clearly support the presence of the direct Zr−Ir bond. Previously reported Ir−Sn bonded species contains terminal hydrides, Cp*Ir(SnMe$_3$)(H)$_3$[18] in contrast to the Zr−Ir hydride-bridged species found here. The Zr−Ir−Cp*(cent) angles are approximately linear (174.9°−176.8°) to arrange the Ir in a three-legged piano stool geometry (excluding the Zr

dx.doi.org/10.1021/ic500258g | Inorg. Chem. 2014, 53, 6634−6654

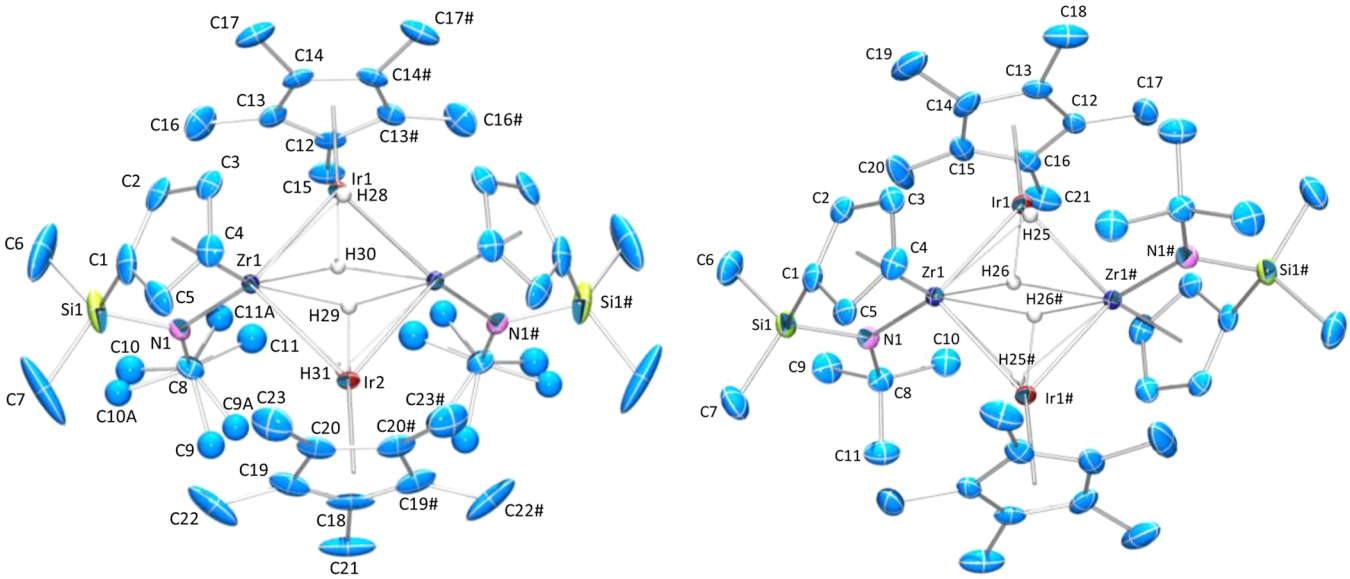

Figure 1. Molecular structures of *syn*-**9** (left) and *anti*-**9** (right). Cyclohexane solvent molecule and hydrogen atoms except for hydride ligands are omitted from both crystal structures for the sake of clarity.

Table 1. Selected Bond Distances and Angles of Planar Square Zr_2Ir_2 Hydrides

complex	*syn*-**9**	*anti*-**9**	**4** (L = Cp)[a]	**4** (L_2 = Bu_2SiCp_2)[a]
		Bond Lengths (Å)		
Zr−Ir	2.7239(3)	2.7299(3)	2.8158(6)	2.7711(6)
	2.7278(3)	2.7253(3)	2.7987(6)	2.7957(5)
Zr−N	2.136(3)	2.122(3)		
Cp(cent)−Zr	2.227	2.221	2.307	2.310
			2.289	2.305
Cp(cent)−Ir	1.939	1.945	1.964	1.951
Zr−H(av)	2.36	2.38	2.43	2.33
Ir−H(av)	1.55	1.66	1.59	1.57
		Bond Angles (deg)		
Zr−Ir−Cp(cent)	140.2	137.04	137.25	137.78
	140.3			
Cp(cent)−Zr−N	100.2	100.85		
Zr−Ir−Zr	79.37(1)	78.13(1)	81.05(2)	81.79(2)
	79.51(1)			
Ir−Zr−Ir	100.53(1)	101.87(1)	98.95(2)	98.21(2)
Ir−Zr−Ir−Zr	1.96(2)	0.00	0.00	0.00

[a]Data taken from ref 12.

atom from the vertices). This has been observed in other related Zr−Ir trihydrido complexes such as **1** and $(Cp^*ZrR_2)(Cp^*Ir)(\mu\text{-}H)_3$ (R = Cl, CH_2SiMe_3).[19] The Zr−C_R lengths (*ca.* 2.30 Å) and Zr−N lengths (*ca.* 2.10 Å) in $(L^1ZrR)(Cp^*Ir)(\mu\text{-}H)_3$ are both slightly longer than Zr−C_{Ph} lengths (av 2.274 Å) and Zr−N length [2.075(4) Å] of mononuclear L^1ZrPh_2 while Cp(cent)−Zr−N bite angles in the L^1Zr framework lie within the typical range (101°−102°).

The three bridging hydride ligands could be well-located and are obviously nonequivalent in each static solid-state structure (see Figure 2 and CIF files in the Supporting Information). However, unlike the crystal structures, they are observed to be equivalent in the ^1H NMR spectra at ambient temperature. A variable-temperature NMR study for **7** in a temperature range from 25 °C to −110 °C showed rapid site exchange of the bridging hydrides (the single resonance of the three hydrides was $w_{1/2}$ = 3.4 Hz at 25 °C, 6.3 Hz at 60 °C, and 12.0 Hz at −110 °C) and nearly nonrestricted rotation about the Zr−C_{Ph} bond (only broadened signals of *ortho*- and *meta*-phenyl protons are observed below −100 °C).[20]

dx.doi.org/10.1021/ic500258g | *Inorg. Chem.* 2014, 53, 6634−6654

Scheme 5. Synthesis of Complexes 10−17 by Organolithium Methods

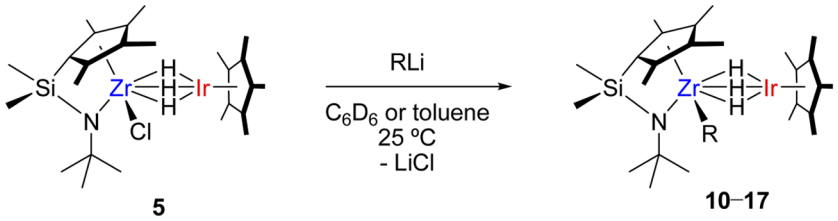

R = alkyl	R = aryl
Me (**10**) (97% yield)	1-naphthyl (**13a**) (95% yield)
Bu (**11**) (n.d.)	2-naphthyl (**13b**) (98% yield)
CH_2SiMe_3 (**12**) (88% yield)	C_6H_3-3,5-Me_2 (**14a**) (97% yield)
	C_6H_3-2,6-$(OMe)_2$ (**15a**) (0% yield)
	C_6H_3-2,4-$(OMe)_2$ (**15b**) (95% yield)
	2-benzofuryl (**16**) (95% yield)
	2-furyl (**17**) (>99% yield)

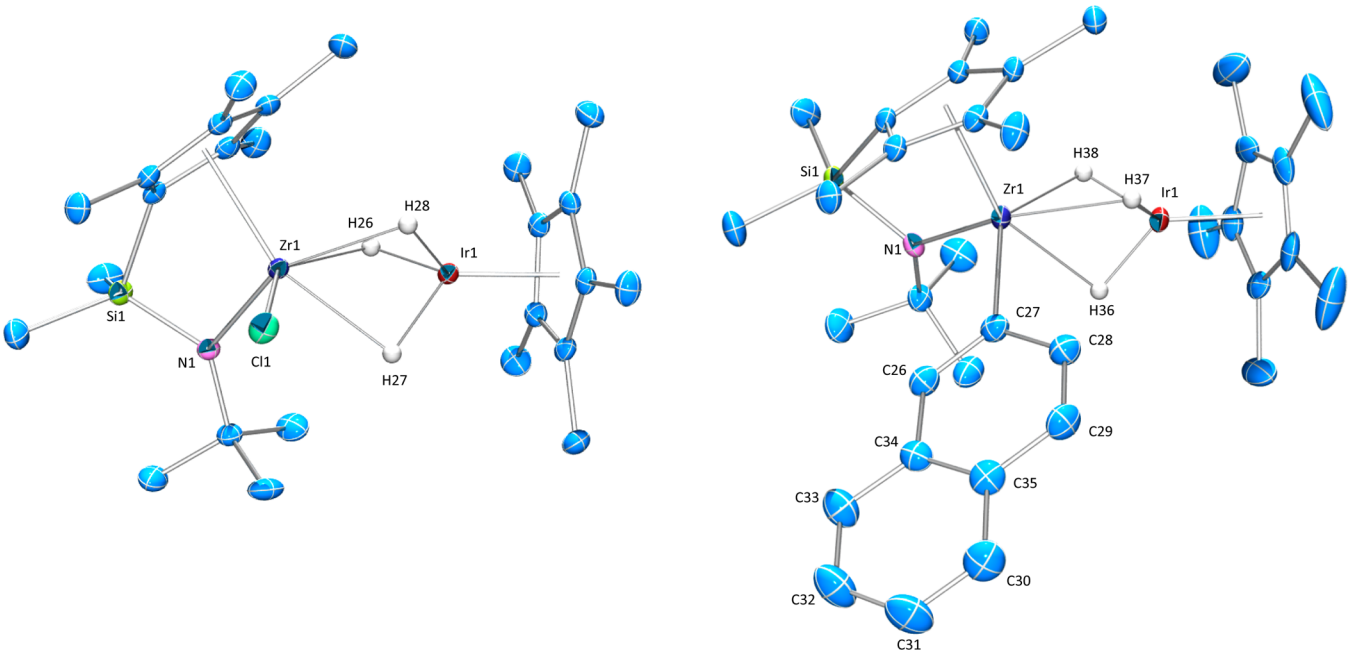

Figure 2. Molecular structures of **5** (left) and **13b** (right). Hydrogen atoms except bridging hydride ligands are omitted for the sake of clarity.

Table 2. Selected Bond Distances (Å) and Angles (deg) of (L^1ZrR)(Cp*Ir)(μ-H)$_3$ (5, 7, 12, 13b, and 17) Obtained by the Organolithium Method

complex	5	7	12	13b	17
		Bond Distances			
Zr−Ir	2.7388(2 Å)	2.7448(3) Å	2.7598(4) Å	2.7447(4) Å	2.7426(5) Å
Zr−Cl or Zr−C_R	2.4422(6) Å	2.296(3) Å	2.298(4) Å	2.302(4) Å	2.291(5) Å
Zr−N	2.101(2) Å	2.106(3) Å	2.102(4) Å	2.105(3) Å	2.103(4) Å
Cp(cent)−Zr	2.199 Å	2.215 Å	2.216 Å	2.202 Å	2.201 Å
Cp(cent)−Ir	1.855 Å	1.858 Å	1.893 Å	1.856 Å	1.859 Å
Zr−H(av)	2.16 Å	2.14 Å	2.19 Å	2.14 Å	2.18 Å
Ir−H(av)	1.58 Å	1.54 Å	1.63 Å	1.55 Å	1.56 Å
		Bond Angles			
Zr−Ir−Cp(cent)	176.55°	175.36°	174.92°	176.75°	176.30°
Cp(cent)−Zr−N	101.08°	102.13°	101.60°	101.71°	101.29°
Ir−Zr−Cl or Ir−Zr−C_R	106.39(2)°	106.31(8)°	108.50(12)°	103.98(11)°	101.82(13)°

dx.doi.org/10.1021/ic500258g | *Inorg. Chem.* 2014, 53, 6634−6654

Table 3. Exchange Reaction of $(L^1ZrR)(Cp^*Ir)(\mu\text{-}H)_3$ with C_6D_6 Solvent[a]

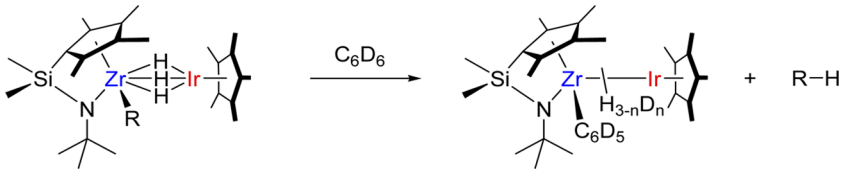

entry	R (complex)	T (°C)	$t_{1/2}$ (h)
1	Ph (**7**)	25	no exchange
2	Ph (**7**)	70	2.6
3	Me (**10**)	50	32
4	Me (**10**)	70	2.2
5	Bu (**11**)	25	125
6	CH_2SiMe_3 (**12**)	80	no exchange
7	CH_2SiMe_3 (**12**)	100	18
8	2-naphthyl (**13b**)	70	3.9

[a]The complex was heated in C_6D_6 (0.01 M, 0.5 mL) at the given reaction temperature until ca. 80% conversion.

Scheme 6. Attempted Methane C−H Activations

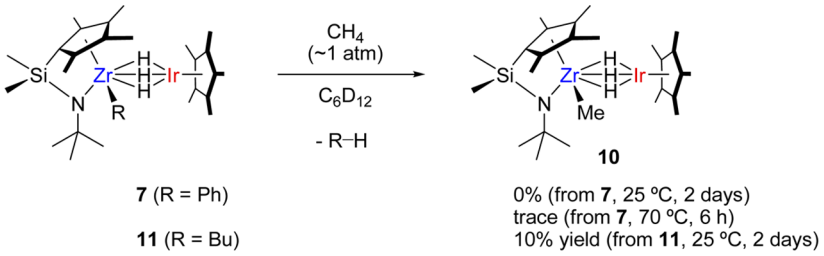

II. Ligand Exchange. *1. Exchange with C_6D_6.* Ligand exchange reaction of **7**, **10**−**12**, and **13b** with C_6D_6 (as an arene substrate and a solvent) was carried out on an NMR scale. As shown in Table 3, these reactions smoothly proceeded under the given reaction conditions, yielding $(L^1ZrC_6D_5)(Cp^*Ir)(\mu\text{-}D)_3$ (**7**-d_8) and the corresponding elimination products.[21] The reactivity order estimated from the observed half-life ($t_{1/2}$) of the starting complexes is **11** (R = Bu) ≫ **10** (Me) > **7** (Ph) > **13b** (2-naphthyl) ≫ **12** (CH_2SiMe_3). This trend obeys the order of the Zr−C bond strengths.[22] It was found that exclusively protio naphthalene was eliminated (corroborated by GC-MS analysis) from **13b** in C_6D_6 solvent (70 °C, 22 h). The fact that no deuterium incorporation into this organic product under the stoichiometric reaction conditions was found unequivocally rules out the possibility that the reaction proceeds via σ-bond metathesis between Zr−R and C_6D_5−D on the early metal side alone. At the same time, they indicate that the reactivity is highly dependent on the hydrocarbyl group at the Zr center in this particular ligand exchange.

2. Ligand Exchange of 7 with Aromatic and Organometallic Substrates. As shown in the former section, the butyl derivative **11** appeared to be thermally unstable to handle. Therefore, we did not address unfunctionalized alkane C−H activation broadly in this work, although the issue of alkane activation is highly challenging.[13,23] Because the methyl derivative **10** appeared to be more thermally stable than **11**, only C−H activation of methane was examined using **11**. A solution of **11** in C_6D_{12} solvent was exposed to methane atmosphere (~1 atm) (see Scheme 6). The reaction progress was monitored at 25 °C by ^{1}H NMR spectroscopy. The formation of **10** was slow but clearly observed under the conditions with competitive decomposition of **11**. In contrast, **7** was likely to reach equilibrium with **10** at 70 °C in 6 h under the methane atmosphere ([**7**]/[**10**] > 50).

On the basis of the above information, i.e., the thermal stability, sufficient reactivity, and solubility of **7** in hydrocarbons, we sought to study the scope and limitation of the ligand exchange of **7** with structurally and electronically divergent aromatic compounds and several organometallic substrates other than C_6D_6 (Table 4).

A variety of aromatic compounds could undergo thermolysis with **7**. Simple aromatic hydrocarbons such as naphthalene and polyalkylated benzenes were primarily tested (entries 1−4). Eliminated benzene can apparently participate in reversible ligand exchange, and in order to obtain better product yields, excess amounts of aromatic substrates were employed but not required as a solvent.[24]

In the presence of naphthalene (ca. 10 equiv), the thermolysis of **7** was conducted at 60−70 °C. Regioselective C−H activation on a naphthalene β-carbon was observed by ^{1}H NMR spectroscopy. The C−H activation reaction is likely to be susceptible to sterically demanding substituents on an aromatic ring. The tendency is further demonstrated by the reaction with 1,3-diisopropylbenzene as well, affording a regioisomerically single product **18** (entry 2 in Table 4). In particular, a class of polymethylated benzenes have chemoselective issues of aromatic versus benzylic methyl C−H activations because of thermodynamic reasons [Ph−H (113 kcal mol^{-1}) versus $PhCH_2$−H (89 kcal mol^{-1})].[25] *m*-Xylene and mesitylene were chosen to simplify the chemoselective issues (entries 3 and 4 in Table 4).

Reaction with *m*-xylene was carried out at 90 °C to give a mixture of isomers **14a** and **14c**, while reaction at 60 °C resulted in slow but exclusive formation of **14a** (after heating for 24 h, **14a** was formed in 45% yield, accompanied by only

dx.doi.org/10.1021/ic500258g | Inorg. Chem. 2014, 53, 6634−6654

Table 4. Ligand Exchange of Complex 7

entry	R–H (equiv)	conditions (°C, h)	product (%yield)	entry	R–H	conditions (°C, h)	product (%yield)
1	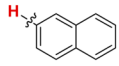 (10.0)	70, 12	**13b** (72)	10	 (3.3)	80, 3	**24** (57)
2	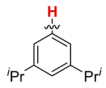 (20.0)	70, 20	**18** (72)	11	 (3.3)	70, 6	**25** (58)
3	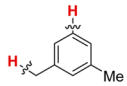 (30.0)	90, 24	**14a**, C_5 (14) **14c**, Bz (57)	12	 (1.2)	70, 20	**26** (84)
4	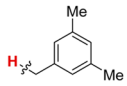 (15.0)	70, 52	**19** (77)	13	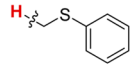 (1.3)	70, 160	**27** (67)
5	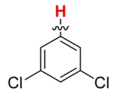 (7.0)	70, 24	**20** (75)	14	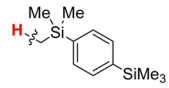 (10.0)	80, 67	**28** (72)
6	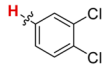 (3.2)	70, 12	**21** (46)	15	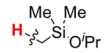 (4.5)	100, 16	**29** (71)
7	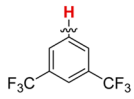 (50.0)	70, 20	**22** (90)	16	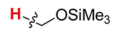 (5.5)	100, 10	**30a** (90)
8	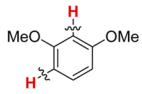 (9.9)	70, 24	**15a**, C_2 (50) **15b**, C_4 (30)	17	 (7.1)	70, 10	**31** (91)
9	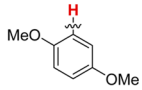 (3.5)	70, 21	**23** (91)	18	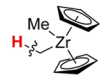 (5.3)	70, 15	**32** (88)

Scheme 7. Proposed Isomerization of 14 through σ-Complex Intermediates

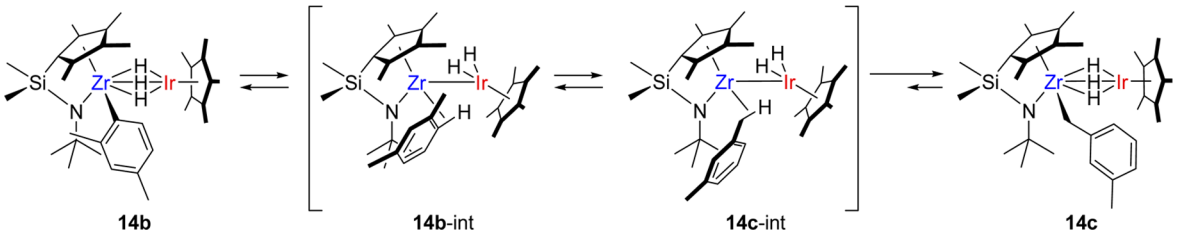

2% of **14c**). Structures of **14a** and **14c** were identified by ^{1}H NMR analysis to be 3,5-dimethylphenyl and 3-methylbenzyl complexes, respectively. Mesitylene was incorporated rather slowly into the bimetallic complex, yielding 3,5-dimethylbenzyl complex **19** with no other isomer. The slow ligand exchange would be attributable to indirect activation of a benzylic methyl C−H bond, i.e., initial activation of the sterically less accessible aromatic C−H bond followed by exchange to the benzylic C−H activation. The structure of **19** was determined on the basis of similarity of the ^{1}H NMR spectrum to that of benzylic complex **14c**. The resonances of the bridging hydrides in **14c** and **19** were observed at δ −14.18 and −14.21 ppm, respectively, which tend to reside between hydride resonances of alkyl and aryl complexes. It is certainly curious to observe no

dx.doi.org/10.1021/ic500258g | Inorg. Chem. 2014, 53, 6634−6654

Scheme 8. Reaction of 7 with 1,3-Dibromobenzene

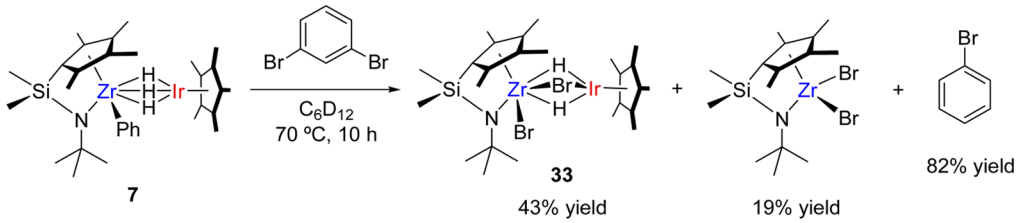

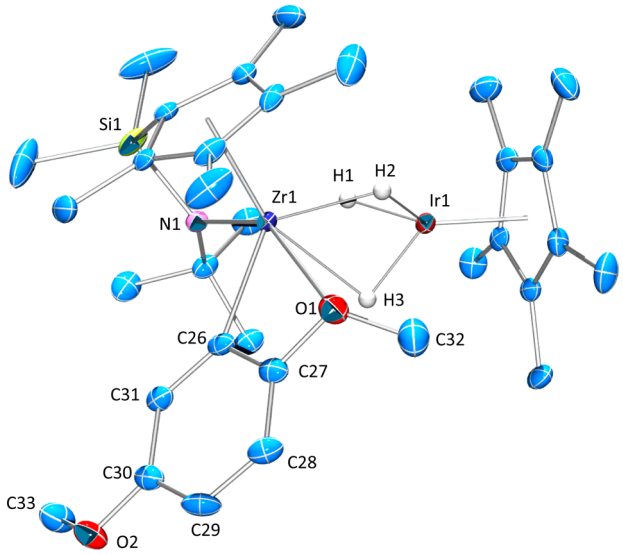

Figure 3. Molecular structure of **23**.

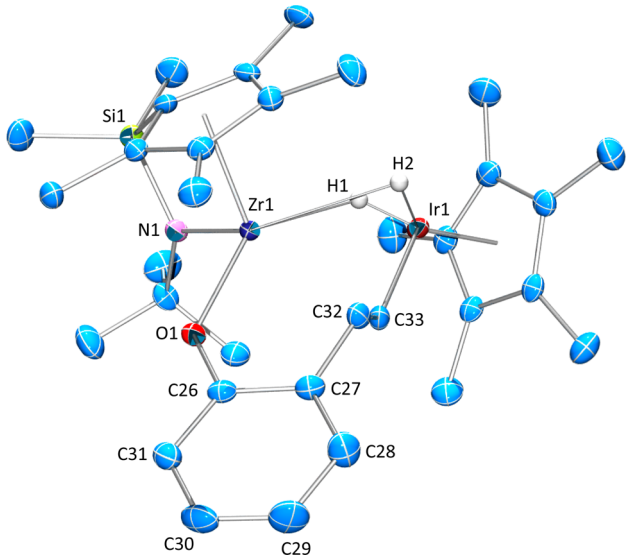

Figure 4. Crystal structure of **35a**.

C−H split in the Cp*Ir fragment of **7**. We attempted reaction with hexamethylbenzene under the similar conditions, but no reaction was observed. To understand the benzylic methyl C−H activations, we also inspected ^{1}H NMR monitoring result of the reaction of **7** and *m*-xylene.

As can be seen from Figure S1 in the Supporting Information, more than 80% of complex **7** was consumed in the initial 1 h with ca. 60% formation of **14a** as a major product while both 2,4-dimethylphenyl complex **14b** and 3-methylbenzyl complex **14c** were detected as minor products (4% and 8% yields, respectively). After 6 h, **14c** became the major product, with a decreased distribution of **14a**. These results suggest occurrence of indirect benzylic C−H activation, most probably via intramolecular isomerization of a σ-complex intermediate (**14b**-int) to another σ-complex (**14c**-int) (see Scheme 7),[26] with the former corresponding structure being intrinsically inaccessible with Cp* and hexamethylbenzene.

Competitive C−H activation versus C−X (X = Cl, Br, I) oxidative addition of haloarenes is particularly interesting, because of potential for polyfunctionalization of aromatic compounds. *Ortho*-selective C−H activations of haloarenes using iridium complexes with pincer ligands were developed.[27] Chloro- and trifluoromethyl-substituted arenes were thus applied to the thermolysis of **7** (entries 5−7 in Table 4), giving rise to the corresponding aryl complexes in moderate to good yields. These results indicate that the functional groups are innocent but serve as sterically hindered groups, resulting in the regioselective C−H activation. In marked contrast, a bromo counterpart, 1,3-dibromobenzene (3 equiv) did not give the corresponding C−H split complex under identical conditions. As shown in Scheme 8, cleavage of Ar−Br bond proceeded, affording the dihydrido complex **33** in 43% yield accompanied by L^1ZrBr_2 (19% yield) and bromobenzene (82% yield, based on **7**). The cleavage of Ar−Br in preference to aromatic C−H activation would be due to the much lower bond enthalpy of Ph−Br (80.4 ± 1.5 kcal mol^{-1}) from those of Ph−H (113 kcal mol^{-1}) and Ph−Cl (95.1 ± 2.5 kcal mol^{-1}).[25]

The structure of **33** was identified by NMR and XRD analysis. Figure S8 in the Supporting Information displays the crystal structure of **33**, which shows the presence of a terminal Zr−Br bond [Zr−Br(av) = 2.625 Å] and a bridging Br ligand [Zr−Br(av) = 2.835 Å, Ir−Br(av) = 2.534 Å]. The structure of **33** does not support Zr−Ir bonding [Zr−Ir(av) = 2.886 Å, FSR = 1.06]. In the ^{1}H NMR spectrum (C_6D_{12} solvent at ambient temperature), resonances of the bridging hydrides are observed to be two nonequivalent broad signals at δ −12.12 ppm ($w_{1/2}$ = 92.8 Hz) and −12.96 ppm ($w_{1/2}$ = 79.0 Hz), exhibiting swift exchange among the bridging ligands. ^{1}H NMR monitoring of the reaction gave no information about any Ir fragments eliminated in the formation of L^1ZrBr_2. At this point, we are not able to determine a clear mechanism for the formation of **33**.

This result led us to further examine reaction of **7** with a nonaromatic organic halide having a weak C−Cl bond such as CCl_4 (BDE: 70.9 kcal mol^{-1}). Similarly, the reaction smoothly proceeded at 80 °C and elimination of benzene was observed. ^{1}H NMR analysis of both C_6D_{12}-soluble and insoluble products and XRD analysis of the C_6D_{12}-insoluble product unequivocally revealed the formation of the ionic pair $[(Cp^*Ir)_2(\mu\text{-}H)_3]$-$[Me_2ClSi(\eta^5\text{-}C_5Me_4)ZrCl_4]$ (**34**) and L^1ZrCl_2, i.e., complete disruption of Zr and Ir fragments (Figure S9 in the Supporting Information). Mechanisms for the formation of the

dx.doi.org/10.1021/ic500258g | *Inorg. Chem.* 2014, 53, 6634−6654

ionic product and cleavage of Zr−N and Si−N bonds remain unclear.

We next performed reaction with other heteroatom-containing substrates such as alkoxyarenes (entries 8 and 9 in Table 4) and pyridine derivatives (entries 10−12 in Table 4). Unlike halogen substituents, these Lewis basic functionalities play an important role in directing regioselection, affording *ortho* C−H split complexes **15**, **23**−**26**.

Crystal structure of **23** is shown in Figure 3. Additional frontal coordination of the proximal methoxy group at the *ortho* position to the Zr center can be seen in the structures of **15a** and **23** [Zr1−O1 = 2.6311(19) Å (**15a**) and 2.8451 Å (**23**)] (see Figure S10 in the Supporting Information). This causes the acute Zr1−C26−C27 angle [104.8(2)° (**15a**) and 109.5(2)° (**23**)], probably reflecting the more coordinatively unsaturated L^1Zr character than zirconocene systems.

Note that dimethylresorcinol gave no *meta*-metalation product but 2,6-dimethoxyphenyl complex **15a** as the major complex, which is not available via the organolithium method as mentioned above (Scheme 5). Regioselectivity of this particular substrate has provided some mechanistic information in C−H activation/functionalization by various late metal systems, i.e., electrophilic late metal complexes often display preference for C−H split at the 4- or 6-position of the aromatic ring, whereas metalation at the 5-position occurs in steric factor-oriented systems.[28] On the other hand, the C^2-metalation product is quite rare and only observed as a minor component in transition-metal systems but as the sole product with main group or lanthanide compounds.[29] The ^{1}H NMR monitoring of the reaction with dimethylresorcinol at 70 °C (see Figure S2 in the Supporting Information) revealed that 2,4-dimethoxyphenyl complex **15b** is more kinetically favored but, after heating for 6 h, the more thermodynamically stable **15a** becomes the major product while no C−H activation at the 5-position was detected throughout the reaction. This observation underlines that the alkoxy group serves as a "directing group" in the present Zr−Ir system.

2,3-Benzofuran has aromatic and vinylic sp^2 C−H bonds, and it is expected to undergo C−H activation at the 2- or 7-position, based on the directing group effect of the ether functionality. The reaction of **7** with an excess amount of benzofuran at 80 °C was monitored by ^{1}H NMR spectroscopy (see Scheme 9). A ^{1}H NMR spectrum of the major product **35a** (75% yield) appeared much different from that of 2-benzofuryl derivative **16** that is accessible from the organolithium method but has two nonequivalent hydrides at δ −14.61 and −15.41 ppm (doublet, J = 8.0 Hz), as well as six proton resonances of C(sp^2)−H in aromatic and vinylic groups (vinylic proton resonances at δ 9.09 and 6.87 ppm with $^3J_{HH}$ = 14.0 Hz). The minor product **35b** has also two nonequivalent hydrides (δ −13.62 and −14.96 ppm with J = 5.2 Hz) and was observed in 10% yield based on integrations for L^1, Cp*, and hydride ligands. Single crystals of **35a** were obtained from pentane. Figure 4 shows the X-ray structure of **35a**, which reveals regioselective $C_{vinylic}$−O bond cleavage in the five-membered ring of benzofuran and *trans* configuration of the vinylic group. The related ring enlargement of an oxygen-containing heterocyclic compound by zirconocene alkyne complexes was reported previously.[30] The Zr−Ir distance [2.9415(3) Å, FSR = 1.08] shows absence of a direct Zr−Ir interaction. In the solid-state structure, the vinylic functionality is located in proximity of the Zr center [Zr1−C32 = 2.660(3) Å, Zr1−C33 = 2.517(3) Å] but the C32−C33 bond length (1.360(4) Å) is in a range of typical C−C double bond lengths, implying no clear interaction between Zr and the vinylic moiety. Based on the ^{1}H NMR spectra of **35b**, the minor product is assignable to be the corresponding (Z)-vinylic isomer (vinylic proton resonances at δ 8.47 and 7.92 ppm with $^3J_{HH}$ = 12.0 Hz).

It is known that a Ni-catalyzed ring-opening reaction of benzofuran with methyl Grignard reagent produces a mixture of (Z)- and (E)-*o*-propenyl phenols and the (Z)-product isomerizes to a 1:3 mixture of the (Z)- and (E)- *o*-propenyl phenols under the catalytic conditions.[31] Pure **35a** appeared to undergo slow partial isomerization to **35b** in solution at ambient temperature. Although the isomerization mechanism is still unclear, we cannot rule out possibility of the mechanism via the η^2-vinyl Ir intermediate described by Crabtree.[32]

Relatively unsatisfactory yields were observed with pyridine and γ-picoline (entries 10 and 11 in Table 4), because of the formation of an unidentified byproduct. In contrast to these pyridine substrates, reaction with 4-dimethylaminopyridine (DMAP) proceeded rather cleanly to afford η^2-pyridyl derivative **26** in high yield (entry 12 in Table 4). The single incorporation of the pyridines should result from the early metal ligand effect; thermolysis of $\{Cp^*Zr(CH_2SiMe_3)_2\}$-$(Cp^*Ir)(\mu\text{-}H)_3$ in the presence of excess pyridines gave bis(pyridyl) complexes containing Zr−C_{py} and Ir−C_{py} bonds,[18] whereas no reaction of the zirconocene−iridium system such as $(Cp_2ZrPh)(Cp^*Ir)(\mu\text{-}H)_3$ with pyridines was observed.

The structure of **26** was established by NMR and X-ray analysis. Despite successful development of the Zr-catalyzed *ortho*-alkylation of pyridines by Jordan and co-workers,[33] only a handful of examples of structurally well-characterized η^2-pyridyl Zr complexes have been reported.[33b,34] In the crystal structure of **26**, there are two independent molecules in the asymmetric unit (Figure 5). These structures are rotamers with respect to the Zr−C bond of the η^2-pyridyl ligation; the pyridyl N atom is coordinated to Zr center in the frontal or lateral site. The latter structure has a slightly bent Zr−Ir−Cp*(cent) = 172.4°; but, in principle, no discernible difference is found in the structural

Scheme 9. Oxidative Addition of Benzofuran $C_{vinylic}$−O Bond

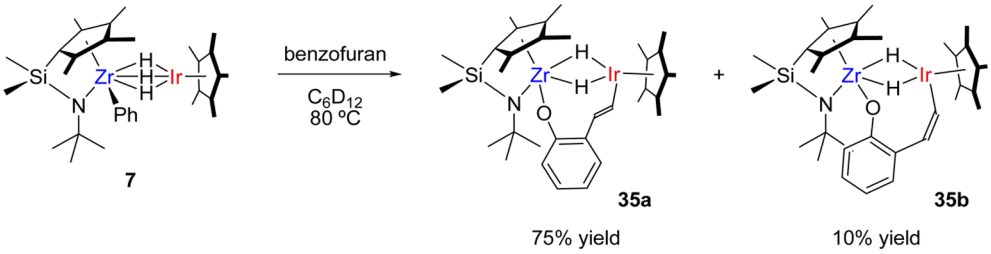

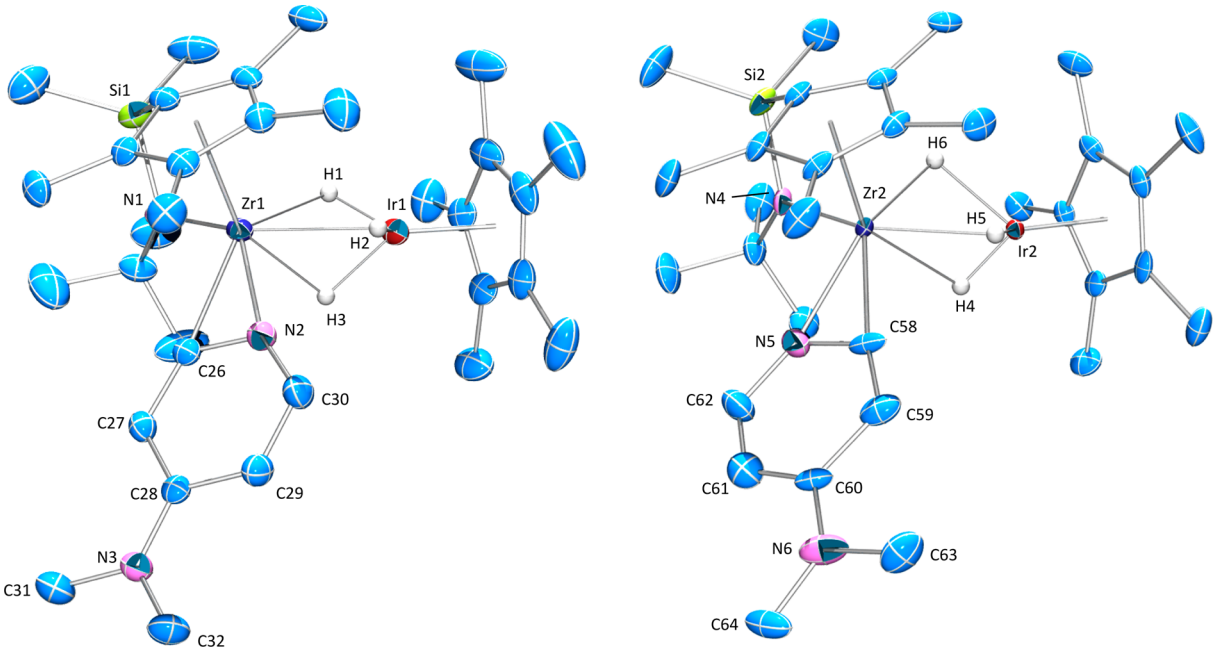

Figure 5. X-ray structures of **26** (two independent molecules in the asymmetric unit). Co-crystallized frontal (left) and lateral (right) rotamers.

Scheme 10. Equilibrium between Rotamers of 26

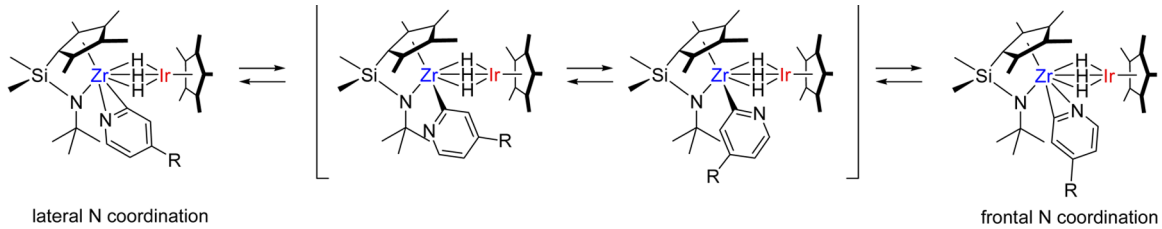

parameters of these rotamers. Krut'ko et al. assigned rotamer structures of $Cp^*_2ZrH(\eta^2\text{-}\kappa C,N\text{-py})$ by NOE and estimated a small barrier for this type of isomerization (ΔG = 1.6 kcal mol^{-1}).[34c] Only one rotamer was observed in the solution ^{1}H NMR spectrum of **26** in C_6D_{12} at ambient temperature, which we assigned by NOESY, HMQC, and HMBC experiments to be the frontal form. These rotamers are likely to have a labile $Zr-N_{Py}$ bond and be in rapid equilibrium in solution after initial formation of the lateral form by bimetallic *ortho* C−H bond cleavage of DMAP (Scheme 10).

Thioanisole was also examined as a heteroatom-containing substrate (entry 13 in Table 4). The thermolytic reaction required a much longer time to obtain a sufficient conversion of **7**, while an initially formed but unidentified intermediate disappeared after 16 h at 70 °C; **27** was then formed as the major product in 67% yield. Based on the ^{1}H NMR spectrum, one thioanisole molecule was incorporated in **27**. Despite the expected role of the thioether moiety as a potential directing group[35] for *ortho* aryl C−H activation, five aromatic protons were clearly observed in the NMR spectrum of **27** (C_6D_6 solvent, a 2:2:1 integration ratio at δ 7.52, 7.13, and 6.92 ppm). This complex was assigned as a SCH_2−H split structure (in marked contrast to alkoxyarenes). This assignment was supported by resonance of $ZrCH_2S$ (δ = 36.7 ppm) in ^{13}C NMR and HMQC spectra, as well as crystallography. The formation of **27** was further verified by organolithium method using **5** and a TMEDA·$LiCH_2SPh$ reagent. The selectivity may be ascribed to the thermodynamic preference of $PhSCH_2$−H (93 kcal mol^{-1}) versus Ph−H (113 kcal mol^{-1}) and $PhOCH_2$−H (ca. 96 kcal mol^{-1}).[25]

As listed in entries 14−18 of Table 4, several organometallic compounds were studied as reaction substrates. The two trimethylsilanes (entries 14 and 15 in Table 4) showed common chemoselectivity, i.e., $SiCH_2$−H activation took place to afford silylmethylated complexes **28** and **29**, respectively. On the other hand, Me_3SiOMe initially gave silylmethylated complex $\{L^1Zr(CH_2SiMe_2OMe)\}(Cp^*Ir)(\mu\text{-}H)_3$ (**30b**) to a significant extent but, after heating at 100 °C for 10 h, this further underwent methyl ether C−H activation, leading to the predominant formation of siloxymethyl complex **30a** in high yield (entry 16 in Table 4). Ferrocene has 10 equivalent aromatic C−H bonds and the reaction with **7** proceeded as smoothly as aromatic hydrocarbons, yielding the corresponding C−H split product **31** (entry 17 in Table 4). However, the reaction of Cp_2ZrMe_2, which has not only 10 equivalent C−H bonds on the Cp rings but also two methyl groups on the Zr atom, gave rise to methyl C−H split complex **32** exclusively (entry 18 in Table 4).

3. Catalytic H/D Exchange. Next, we anticipated that catalytic H/D exchange between arenes and C_6D_6 could provide more information about which C−H bond can be split by the bimetallic complex. NMR-scale exchange between several arenes and C_6D_6 as solvent was carried out at 120 °C in the presence of catalytic amounts of **7**, and these results are listed in Table 5. Total deuterium incorporations into arenes, regioselections, and d_n distributions were estimated by NMR

Table 5. 7-Catalyzed H/D Exchange between Arenes and C_6D_6[a]

entry	arene ($[arene]_0/[7]_0$)[b]	time (h)	total D into Ar-H (%)[c]	regioselection[b]
1	C_6H_4-1,3-$_i$Pr$_2$ (118)	100	22	H^5 (81%) ≫ H^4, H^6, H^2
2	C_6H_4-1,3-$(CF_3)_2$ (129)	15	26	H^5 (>99%)≫ H^4, H^6, H^2
3	$C_{10}H_8$ (48)	113	53	H^β (83%) ≫ H^α
4	$C_{10}H_7$-1-OMe (40)	100	48	H^3 (90%), H^6, H^7 ≫ H^4, H^5 > H^8 > H^2
5	$C_{10}H_7$-2-OMe (40)	114	55	H^3 (93%), H^6, H^7 ≫ H^4, H^5, H^8 > H^1

[a]NMR-scale reaction of **7** and the given arene was carried out in C_6D_6 (0.6 mL) at 120 °C. [7] = 0.006−0.01 M. [b]As determined by ^{1}H NMR analysis. [c]As determined by comparison with the starting arene samples in GCMS analysis.

Scheme 11. C−H Activation of 1-Methoxynaphthalene in C_6D_6

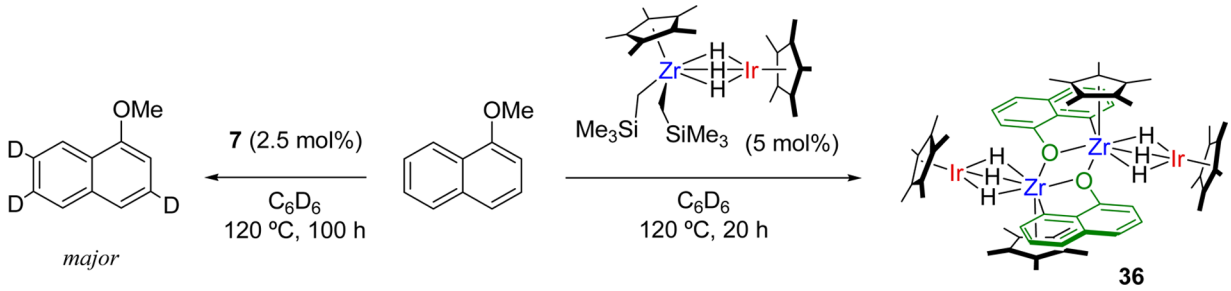

and GC-MS analysis. In each reaction, **7**-d_8 was detected in the NMR spectra throughout the H/D exchange. Therefore, we considered that a dinuclear Zr−Ir species serves as an active catalyst and the regioselective outcomes in the catalytic H/D exchange should, in principle, follow those in the stoichiometric reactions.

In fact, the observed selectivities in the catalytic H/D exchange are fairly consistent with those expected from the regioselective C−H bond cleavage of the substrates tested (1,3-diisopropylbenzene, 1,3-bis(trifluoromethyl)benzene, naphthalene, and methoxyarenes) with **7** under the milder conditions (Table 4). Nevertheless, the results in Table 5 indicate that activation of sterically less accessible C−H bonds also occur under more forcing conditions; albeit the lower deuterium incorporations. A significant degree of deuterium incorporations (ca. 23%) into α-C−H of naphthalene was observed (entry 3 in Table 4).

When the previously reported $\{Cp^*Zr(CH_2SiMe_3)_2\}$-$(Cp^*Ir)(\mu\text{-}H)_3$[19] was employed with 1-methoxynaphthalene under the identical H/D exchange conditions, chelating complex **36** was formed via C^8−H and Me−O bond cleavages, and no further H/D exchange occurred after 20 h (see Scheme 11 and Figure S11 in the Supporting Information). Cleavage of C−O bond of alkyl ethers was achieved by bis(indenyl)-zirconium sandwich complexes and half-sandwich zirconocene hydroborate-$B(C_6F_5)_3$ system under mild conditions.[36] On the other hand, replacement of the Zr ligand to the *ansa*-cyclopentadienyl-amide L^1 retained the uniform catalyst activity, yielding the corresponding deuterium-enriched aromatic compounds (entry 4 in Table 5). Despite the favored *ortho* C−H bond cleavage of heteroatom-containing arenes (entries 8−12 in Table 4), exchanges in C^2−H bond of 1-methoxynaphthalene and C^1−H bond of 2-methoxynaphthalene were both completely interfered, presumably, by the steric repulsion between the ligand L^1 and the naphthyl ring. Unlike the cases of PhSMe and Me_3SiOMe, methyl ether C−H bonds in the aromatic substrates did not participate to H/D exchange, even at 120 °C.

III. Attempted Isolation of Zr−Ir Bonded Species. *1. Thermolysis of 7 in the Presence of X- and L-Type Ligands.* To explore the possibility of formation of Zr−Ir bonded intermediates, we attempted thermolytic reactions of **7** with various ligands. The proposed transient complex, i.e., $(L^1Zr)(Cp^*IrH_2)$, after benzene elimination from **7**, was expected to coordinate with certain Lewis bases such as heteroatom-containing ligands. We suggest that these coordinate in the initial step of the regioselective C−H activations of methoxyarenes and pyridines, which were experimentally observed (see Table 3). Therefore, we attempted to trap this species with Lewis bases, which would not undergo C−H activation. However, PMe_3 and THF were ineffective at trapping the transient species, resulting in the formation of intractable materials.

These failures led us to turn to the use of a halide as an X-type ligand or a relatively strong oxo base as an L-type ligand that are hoped to stabilize the Lewis acidic Zr center. Reaction of **7** with $Bu_4N^+Br^-$ in THF-d_8 at 80 °C led to the moderately clean formation of a new complex **37** (67% NMR yield based on L^1 ligand integration), along with a small amount of $(L^1ZrBr)(Cp^*Ir)(\mu\text{-}H)_3$ (**5′**) (Scheme 12). The ^{1}H NMR spectrum of crude **37** contains resonances of both C_1-symmetric L^1 fragment and Cp* ligand over slightly wide chemical shift region of Me groups in L^1 ($CpMe_4$: δ 2.63−1.71 ppm; $SiMe_2$: δ 0.41 and 0.26 ppm), as well as a hydride resonance (δ −13.90 ppm). These characteristic chemical shifts are observed similarly to those of phosphine oxide adducts **39** (shown later). **37** was found to be a dihydrido complex and undergo no H/D exchange with THF-d_8 under the reaction conditions. Separation of **37** from the remaining $Bu_4N^+Br^-$ was impaired by their similar solubility and poor crystallinity. Cleaner formation of **37** was attained via the use of an excess of **7** (1.4 equiv, 90% NMR yield based on $Bu_4N^+Br^-$). However, **37** seems to gradually decompose during the course of recrystallization, resulting in the butylation of the Ir center with Bu_4N^+, i.e., formation of neutral butyl dihydrido complex $(L^1ZrBr)(Cp^*IrBu)(\mu\text{-}H)_2$ (**38**) (see Figure S12 in the Supporting Information).[37] Therefore, the structure of **37** was temporarily assigned as drawn in Scheme 12, based on the similarity of the ^{1}H NMR data to that of fully characterized **39b**.

Scheme 12. Reaction of 7 and $Bu_4N^+Br^-$

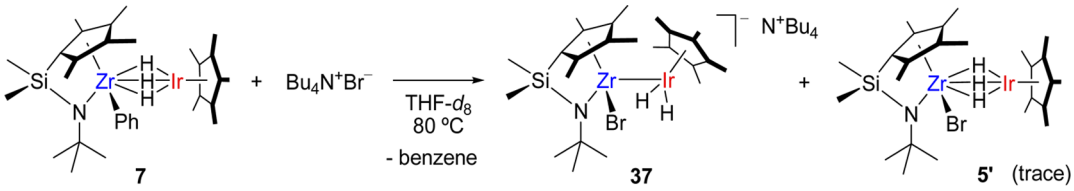

Phosphine oxides are known to effectively stabilize Lewis acidic metal centers, such as early transition metals, lanthanides, and actinides, whose Lewis acid−base adducts have been well-characterized.[38] Next, we addressed the thermolysis of **7** at 80 °C in the presence of several commercially available phosphine oxides R_3PO (R = Me(**a**), Et(**b**), Bu(**c**)) as L-type ligands; these results are summarized in Scheme 13 and Table 6.

Scheme 13. Formation of 39

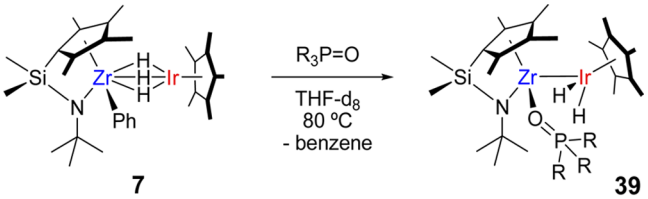

R = Me (**a**), 25% yield
Et (**b**), 87% yield
Bu (**c**), 86% yield

Table 6. ^{31}P NMR data of R_3P═O and Their Adducts (Solvent: THF-d_8)

R	chemical shift (δ/ppm)[a]		
	free R_3P═O	adduct	
Me	32.3	**39a**	63.8
Et	46.1	**39b**	73.4
		$TiCl_4$·$OPEt_3$	72.7[b]
		$SnCl_4$·$OPEt_3$	67.4[b]
Bu	42.3	**39c**	69.1

[a]Referenced to 85% H_3PO_4 in D_2O. [b]Data taken from ref 41 (solvent: ether).

Among the phosphine oxides tested in this study, ethyl and butyl derivatives led to the clean formation of the desired adducts **39b** and **39c**, respectively. **39b** and **39c** are soluble in pentane, and **39b** was isolated as pure crystals, whereas the high solubility of **39c** prevented isolation. In contrast, Me_3PO gave an unsatisfactory result with only a small amount of the corresponding adduct **39a** detected by ^1H NMR analysis. It was not possible to improve the yield higher than 25%, with the formation of an unidentified byproduct always observed despite the reaction conditions (the temperature, reaction time, and amounts of Me_3PO).[39]

The Gutmann acceptor number (AN) is used for quantitative measurement of Lewis acidity in a variety of solvents.[40] The AN is based on the ^{31}P NMR chemical shift of Et_3PO as a probe molecule. From the data for **39b** in Table 6, the Gutmann AN for the ligand-free transient species is estimated to be 64. As a result, the Zr center is thought to have Lewis acidity in a region between $TiCl_4$ (AN = 70) and $SnCl_4$ (AN = 59),[41] and helps to account for the above regioselective C−H activation of N- and O-containing substrates (see Table 4).

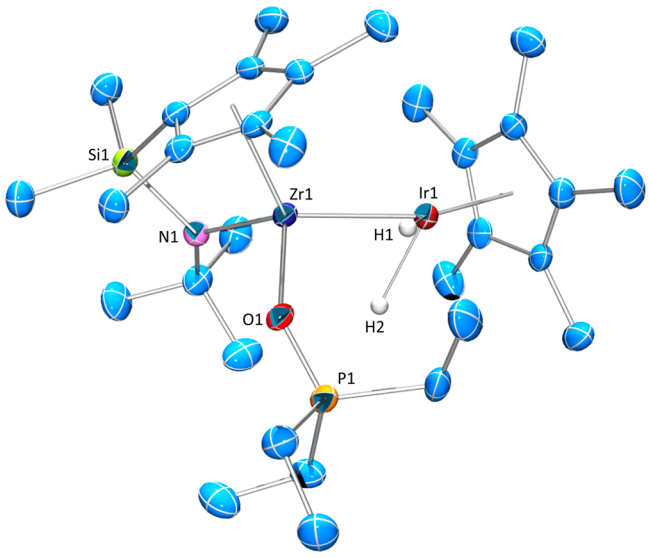

Figure 6. X-ray structure of **39b**. Hydrogen atoms (except Ir−H) are omitted for the sake of clarity. Selected bond lengths (Å) and angles (deg): Zr1−Ir1, 2.5491(4) Å; Zr1−N1, 2.149(3) Å; Zr1−O1, 2.156(3) Å; P1−O1, 1.517(3) Å; Zr1−Cp(cent), 2.246 Å; and Ir1−Cp(cent), 1.931. Zr1−Ir1−Cp(cent), 161.33°; O1−Zr1−Ir1v, 105.97(7)°, N1−Zr1−Ir1, 112.46(9)°; Ir1−Zr1−Cp(cent) , 122.77°; N1−Zr1−Cp(cent), 101.16°; and O1−Zr1−Cp(cent), 105.04°.

*2. Structure of **39b**.* Complex **39b** was recrystallized from pentane at −10 °C, affording an orange chunk. The structure was determined by X-ray analysis (Figure 6). The molecular structure may be contrasted with those of the trihydrido complexes in Figure 2. The Zr−Ir distance of **39b** is substantially contracted to 2.5491(4) Å, the FSR being 0.938.[17] The Zr−Ir distance is significantly shorter than that of the reported Zr−Ir single bonds (2.60−2.64 Å).[7] The P−O bond length [1.517(3) Å] is comparable to those of free tertiary phosphine oxides.[42] The bending angle Zr−Ir−Cp*(cent) = 161.3° indicates that the Zr atom occupies one of the vertices of the distorted tetrahedron of the Ir geometry, likely facilitating stronger Zr−Ir interactions. Two hydride ligands could be well-located in the difference-Fourier map and could be refined. The Zr−IrH_2 core structure is comparable with the recently reproted {Cp*Ta(CH_2SiMe_3)$_2$}(Cp*IrH_2) [Ta−Ir = 2.4457(3) Å, Ta−Ir−Cp*(cent) = 163.7°].[11] The long H1−H2 distance (>2.1 Å), as determined by the X-ray analysis and the spin−lattice relaxation time for the hydride resonance (T_1 > 460 ms) rule out **39b** as a nonclassical hydrido complex (see Figure S3 in the Supporting Information).

The ^1H NMR spectrum of **39b** shows a single resonance for the two hydride ligands at ambient temperature, although they are nonequivalent hydrides in the solid state. Therefore, we examined a VT-NMR study for **39b** (Figure 7). The hydride resonance appeared as a single peak at a temperature higher than −60 °C, began broadening at −80 °C, and ultimately

dx.doi.org/10.1021/ic500258g | Inorg. Chem. 2014, 53, 6634−6654

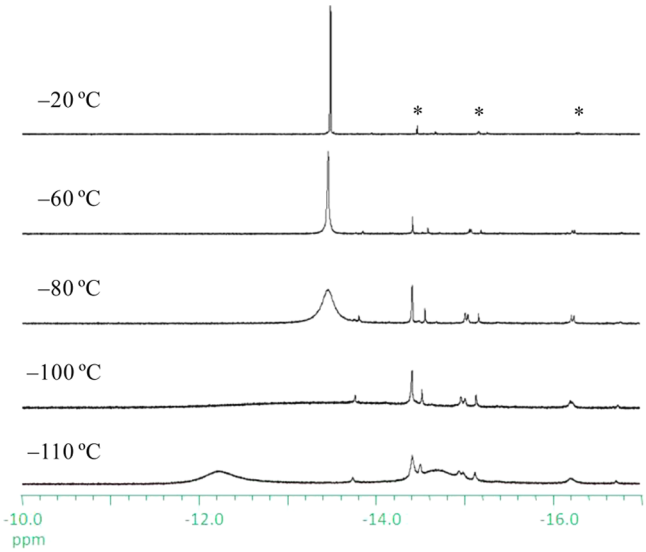

Figure 7. VT-NMR spectra of **39b** (hydride region). The asterisks denote impurities.

decoalesced at −110 °C into two broad signals at δ −12.22 and −14.69 ppm (1:1). The hydride site exchange likely proceeds via oscillation between terminal and bridging hydride structures; this process may alter the Zr−Ir interactions to a significant extent. The IR spectrum of **39b** includes characteristic absorption bands at 2154 and 1244 cm^{-1}, the former absorption is assigned to terminal Ir−H stretching vibration and the latter is ν(PO). Based on these data we would conclude that the proposed Zr−Ir bonded structure with terminal hydrides has a major contribution to the structure of **39b**.

IV. Mechanism through Zr−Ir Bonded Intermediates.

1. Proposed Mechanism. We considered the likelihood that C−H activation of **7** involves Zr−Ir directly bonded intermediates such as σ-arene, σ-alkane complex, and ligand-free transient species analogous to the well-defined {Cp*Ta-$(CH_2SiMe_3)_2$}(Cp*IrH_2),[11] a postulated mechanism for the (reversible) reaction between $\mathbf{I}_{R1}$ and R^2−H is displayed in Scheme 14. As mentioned in the above section (exchange between C_6D_6 and complexes **7**, **10**−**12**, and **13b**, see Table 3), the reactivity for the ligand exchange can vary, depending on the combination of R^1 group in $\mathbf{I}_{R1}$ and substrate R^2 group for different Zr−C bond strengths[22] and the number of accessible C−H bonds. The proposed mechanism is as follows. The reaction is initiated from reductive coupling of $\mathbf{I}_{R1}$ to form a σ-complex intermediate $\mathbf{II}_{R1}$, followed by ligand dissociation to give a ligand-free intermediate **III**. In turn, coordination of an external ligand R^2−H to the *endo*-dihydride **III** affords another σ-complex intermediate $\mathbf{II}_{R2}$, and finally oxidative cleavage of the C−H bond provides the product $\mathbf{I}_{R2}$. Here, we define two dihydride orientations on the Ir with respect to L^1Zr geometry in $\mathbf{II}_{R1}$ and $\mathbf{II}_{R2}$ as *exo*-form and in **III** as *endo*-form (These forms for **II** and **III** are based on the DFT results, shown later). Moreover, in the presence of phosphine oxide, Lewis acidic **III** could be trapped to form *endo*-dihydride **39**. The process is irreversible and the kinetic study for the reaction of **7** to **39b** may also provide useful information.

Apparently, both the reductive elimination and oxidative addition involve a process which is neither associative nor dissociative, i.e., $\mathbf{I}_{R1} \rightarrow \mathbf{II}_{R1}$ and $\mathbf{II}_{R2} \rightarrow \mathbf{I}_{R2}$, while the dissociative process $\mathbf{II}_{R1} \rightarrow \mathbf{III}$ and the associative process $\mathbf{III} \rightarrow \mathbf{II}_{R2}$ are also contained in the proposed exchange mechanism. Activation parameters obtained and kinetic isotope effects (KIEs) observed in the following kinetic studies may address which process is the rate-determining step, although the key step can be altered, depending on the reactants employed. In this kinetic study, we decided to exploit **7** and **10** as starting complexes **I**.

2. Kinetic Study for Ligand Exchange. Several groups have reported comprehensive studies on mechanisms and KIEs in alkane and arene C−H bond activation mediated by transition-metal alkyl and aryl hydrido complexes featuring cyclopentadienyl ligands.[43−45] In our system, we attempted the synthesis of $(L^1ZrPh)(Cp^*Ir)(\mu\text{-}D)_3$ (**7**-d_3) from (L^1ZrCl)-$(Cp^*Ir)(\mu\text{-}D)_3$ (**5**-d_3) (>99% D incorporation) in toluene solvent at 25 °C. However, because of the presence of the three bridging deuterides in once formed **7**-d_3, a rather complicated mixture of **7**-d_3 isomers, i.e., $\{L^1Zr(C_6D_nH_{5-n})\}(Cp^*Ir)(\mu\text{-}D)_{3-n}(\mu\text{-}H)_n$ (n = 0−3) was observed, namely, the intramolecular H/D scrambling seemed to occur much more rapidly at the temperature than the intermolecular exchange with the solvent; in fact, no isomers of predictable tolyl and benzyl derivatives were formed. The desirable **7**-d_3 could not be synthesized cleanly. Thus, we decided to employ naphthalene(-d_8) as a labeled arene substrate, which we regard to be relatively close to benzene compared to other arene substrates in terms of the number of the sterically equivalent accessible hydrogens (four vs six) and the C−H bond strength (111.9 ± 1.4 kcal mol^{-1} vs 112.9 ± 0.5 kcal mol^{-1}).[25] Also, complex **7** shows a ^{1}H NMR spectrum distinctive from that of **13b**, which is helpful in performing the kinetic studies utilizing NMR spectrometry.

The reaction of **7** with naphthalene is reversible (Scheme 14), and the equilibrium lies on the side of **13b** in the presence of excess naphthalene. We simply used a large excess of naphthalene to measure pseudo-first-order rate constants. In the presence of >10 equiv of naphthalene, the reaction plots nicely fit first-order kinetics in [**7**] at least 60% conversion (see Table 7 and Figure S4 in the Supporting Information),[46] while a reduced amount of naphthalene decreased the reaction rate (entries 3 and 4 in Table 7). Based on the k_{obs} (see entries 1−3, 6, and 7 in Table 7), activation parameters were estimated for the exchange reactions of **7** with naphthalene to be $\Delta H^{\ddagger}$ = 28.7 ± 0.5 kcal mol^{-1}, $\Delta S^{\ddagger}$ = 6.9 ± 1.3 eu, and $\Delta G_{298}{}^{\ddagger}$ = 26.6 ± 0.8 kcal mol^{-1} (Figure 8). The small value of $|\Delta S^{\ddagger}|$ indicates two possibilities: (i) the rate-determining step is involved in either a unimolecularly C−H bond forming or breaking process, namely **7** → $\mathbf{II}_{Ph}$ or $\mathbf{II}_{Naph}$ → **13b**, and (ii) the dissociative and associative processes ($\mathbf{II}_{Ph}$ → **III** and **III** → $\mathbf{II}_{Naph}$) in the proposed mechanism have energetically similar level of the transition states, because of the almost-identical reactivity of benzene and naphthalene. In addition, we obtained rate constants using **7** and naphthalene-d_8 (see entry 5 in Table 7) or using $(L^1ZrC_6D_5)(Cp^*Ir)(\mu\text{-}D)_3$ (**7**-d_8) and naphthalene (see Table S2 in the Supporting Information), giving significant estimated KIEs (353.1 K) = 1.25(2) and 0.78(1), respectively. The latter kinetic measurements using **7**-d_8 and naphthalene (see Table S2 and Figure S5 in the Supporting Information) provide activation parameters similar to the above: $\Delta H^{\ddagger}$ = 29.2 ± 0.6 kcal mol^{-1}, $\Delta S^{\ddagger}$ = 8.7 ± 1.6 eu, and $\Delta G_{298}{}^{\ddagger}$ = 26.6 ± 1.1 kcal mol^{-1}. These data imply that the exchange rates depend upon unimolecular C−H(D) bond formation of eliminating organic ligands or C−H(D) bond cleavage of incoming organic molecules.

As mentioned above, unlike the reaction of aryl complexes such as **7** with methane, methane C−H activation was clearly

Scheme 14. Proposed Mechanism for the Reversible Ligand Exchange through Zr−Ir Bonded Intermediates and Formation of 39b

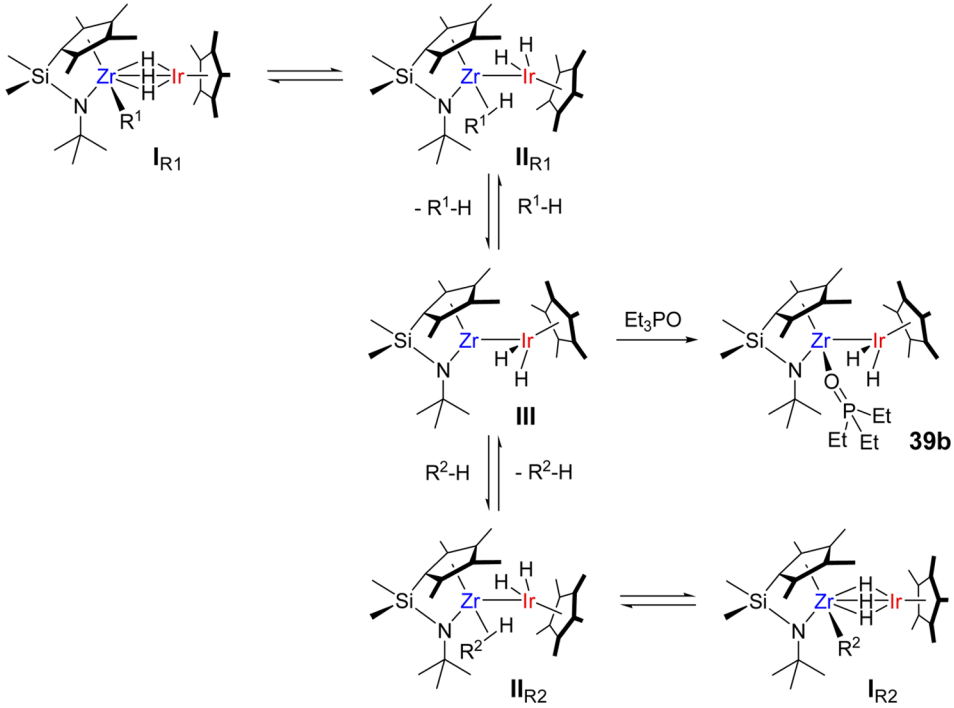

Table 7. Pseudo-First-Order Rate Constants for the Reaction of 7 with Naphthalene[a]

entry	$[C_{10}H_8]_0/[7]_0$	T (K)	k_{obs} ($\times 10^4$ s^{-1})
1	10.5	333.15	0.269 ± 0.002
2	14.6	347.64	1.79 ± 0.01
3	14.6	352.67	3.37 ± 0.02
4	3.1	353.09	3.04 ± 0.04
5[b]	14.6	353.09	2.70 ± 0.04
6	14.6	357.64	5.79 ± 0.04
7	14.6	362.41	9.48 ± 0.12

[a]The reaction was carried out $[7]_0$ = 9.7 mM in C_6D_{12} under the given reaction conditions and monitored by ^{1}H NMR analysis at least until 60% conversion was achieved. [b]Naphthalene-d_8 was used.

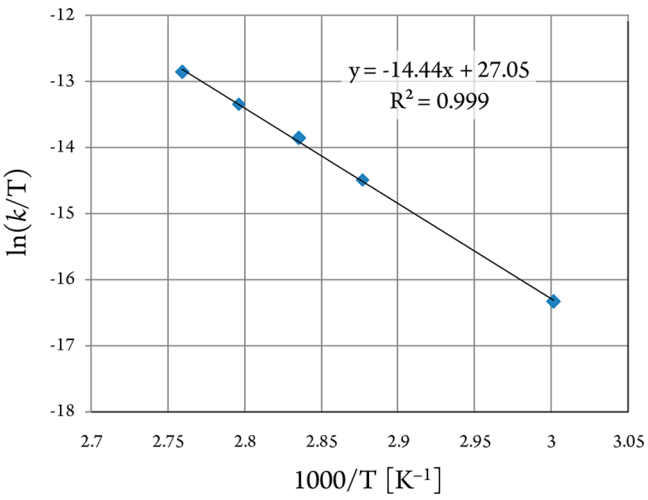

Figure 8. Eyring plot for the reaction of 7 and naphthalene.

Table 8. Pseudo-First-Order Rate Constants for the Reaction of 10 with Naphthalene[a]

entry	T (K)	k_{obs} ($\times 10^4$ s^{-1})
1	333.15	0.259 ± 0.003
2	338.15	0.437 ± 0.002
3	342.88	1.14 ± 0.01
4	347.89	1.98 ± 0.01
5	352.98	3.54 ± 0.03
6	357.85	5.91 ± 0.05
7	362.97	9.64 ± 0.06

[a]The reaction was carried out using $[\mathbf{10}]_0$ = 7.9 mM in C_6D_{12} and $[\text{naphthalene}]_0/[\mathbf{10}]_0$ = 11.0 at the given reaction temperature and monitored by ^{1}H NMR analysis at least until 55% conversion of complex **10**.

Table 9. Pseudo-First-Order Rate Constants for the Reaction of 7 and Et_3PO[a]

entry	$[Et_3PO]_0/[7]_0$	T (K)	k_{obs} ($\times 10^4$ s^{-1})
1	0.60	357.04	4.67 ± 0.02
2	1.05	357.04	4.68 ± 0.02
3	5.56	357.04	4.68 ± 0.03
4[b]	10.74	357.04	4.41 ± 0.03
5[c]	2.44	339.15	0.485 ± 0.005
6	1.48	346.86	1.45 ± 0.01
7	1.48	351.48	2.50 ± 0.01
8	1.48	356.87	4.47 ± 0.03
9	1.48	361.58	7.23 ± 0.05

[a]The reaction was carried out using complex 7 in THF-d_8 ($[7]_0$ = 9.5 mM) at the given temperature and monitored by ^{1}H NMR analysis at least until second half-lives of 7. [b]After 1 h, 81% conversion of 7 and 43% yield of **39b** were observed by ^{1}H NMR assay. [c]Heated in an oil bath.

dx.doi.org/10.1021/ic500258g | Inorg. Chem. 2014, 53, 6634−6654

Table 10. Geometrical Parameters (Bond Lengths and Bond Angles) of Optimized Complexes I_R, II_R, III, and 39b[a]

complex	7	10	12	13b	13b′	II_{Ph}	II_{Me}	II_{Naph}	III	39b
				Bond Lengths (Å)						
Zr−Ir	2.805 (2.1)	2.817	2.811 (1.8)	2.802 (2.1)	2.804	2.516	2.498	2.512	2.476	2.530 (0.8)
Zr−N	2.115 (0.4)	2.123	2.126 (1.1)	2.116 (0.5)	2.113	2.126	2.124	2.131	2.128	2.158 (0.4)
Zr−C_R or Zr−O	2.282 (0.6)	2.271	2.289 (3.9)	2.282 (0.9)	2.285	2.830	2.942	2.824		2.197 (1.9)
Zr−H(av)	2.27 (5.6)	2.27	2.27 (3.5)	2.26 (5.6)	2.27	2.28	2.31	2.29	2.34	2.39 (5.8)
Ir−H(av)	1.64 (5.8)	1.63	1.63 (0.0)	1.63 (5.2)	1.63	1.65	1.65	1.65	1.66	1.64 (4.4)
H−H						2.28	2.29	2.27	2.24	2.25 (4.1)
Cp(cent)−Zr	2.261 (2.0)	2.268	2.275 (2.6)	2.262 (2.7)	2.261	2.281	2.289	2.286	2.247	2.292 (2.0)
Cp(cent)−Ir	1.960 (5.2)	1.960	1.961 (3.5)	1.960 (5.6)	1.963	2.050	2.053	2.055	2.057	2.066 (6.5)
				Bond Angles (deg)						
Zr−Ir−Cp(cent)	178.8 (1.9)	178.5	177.2 (1.3)	178.9 (1.2)	179.1	162.3	159.6	161.8	155.5	156.3 (3.2)
Cp(cent)−Zr−N	100.7 (1.4)	100.7	100.4 (1.2)	100.6 (1.1)	100.7	99.8	99.8	99.6	100.9	99.7 (1.5)

[a]Values given in parentheses show the percentage deviation from the experimental values.

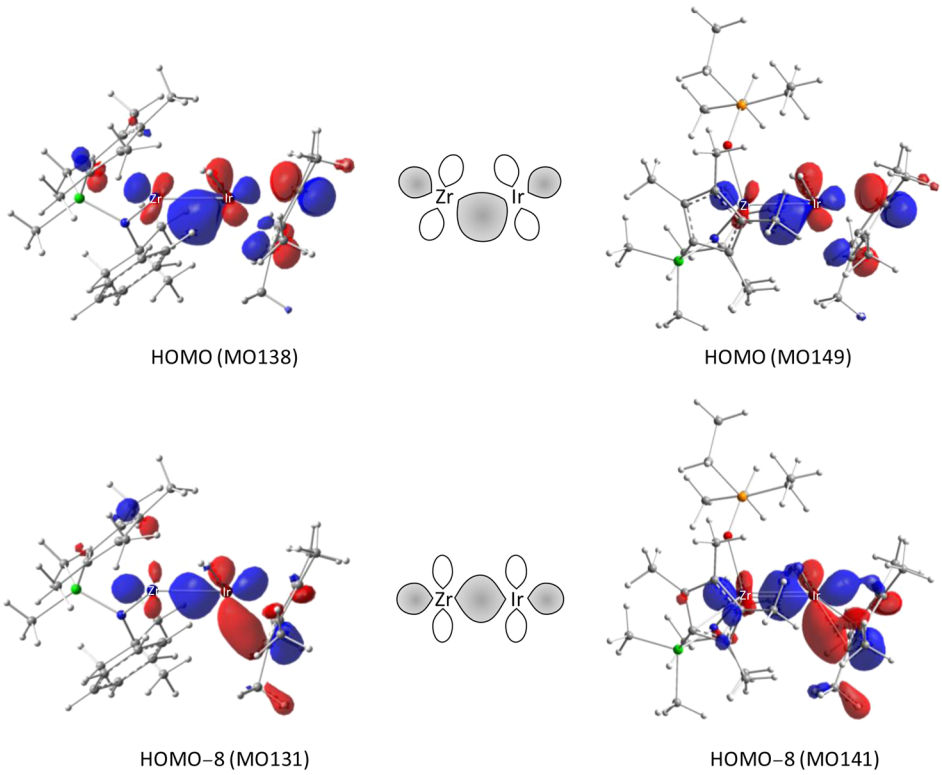

Figure 9. Zr−Ir bonding molecular orbitals for optimized II_{Ph} (left) and **39b** (right) and schematic atomic orbital overlaps between Zr and Ir (center).

observed by using butyl derivative **11**. This should be ascribed to the large difference in reaction rates of proposed **III** toward methane and arene C−H bonds. Thus, we anticipated that II_{Me} lay higher in energy than II_{Naph}, and so, the step of II_{Me} → **III** would be nearly irreversible in the exchange of **10** and excess naphthalene. Therefore, a kinetic study using **10** and naphthalene would more clearly explain about whether the rate-limiting step is **10** → II_{Me} or II_{Me} → **III**. As for the reaction of **7** and naphthalene, kinetic plots for the conversion of **10** in the presence of excess naphthalene (11.0 equiv) in C_6D_{12} solvent showed that the rate law could be approximated as first-order in [**10**] (see Table 8). Since the data obtained at the lower temperatures were deviated (entries 1 and 2),[21] the activation parameters were obtained from the Eyring plot using the rate constants at 343−363 K: $\Delta H^{\ddagger} = 25.8 \pm 0.3$ kcal mol^{-1}, $\Delta S^{\ddagger} = -1.2 \pm 0.9$ eu, and $\Delta G_{298}{}^{\ddagger} = 26.2 \pm 0.6$ kcal mol^{-1} (entries 3−7 in Table 8 and Figure S6 in the Supporting Information). The small $|\Delta S^{\ddagger}|$ may indicate the proposed reductive coupling process **10** → II_{Me} to be the rate-limiting step.

*3. Kinetic Study of the Formation of **39b**.* Kinetic study of the formation of **39b** was carried out in THF-d_8 solvent since Et_3PO appeared to be the better trapping agent for the proposed **III**. One may think that the reaction obeys second-order kinetics in [**7**] and [Et_3PO], i.e., rate = k[**7**][Et_3PO]. We primarily performed the reaction at 357 K with varied ratios of $[Et_3PO]_0/[7]_0$ (from 0.60 to 10.74). The natural logarithm of $[7]/[7]_0$, as a function of time, was found to have linearity, and the rate law was thus regarded as pseudo-first-order in [**7**]; as a result, the rate constants (k_{obs}) were almost uniform at this temperature, irrespective of $[Et_3PO]_0/[7]_0$ ratio (entries 1−4 in Table 9). This implies that the associative step of **III** and Et_3PO

is not the rate-determining step. The use of a large excess of Et_3PO (>10 equiv) or relatively high reaction temperature reproducibly caused undesired side reactions to a considerable extent. C_6D_{12} can also be used as a reaction solvent with more-soluble Bu_3PO reagent but slightly decreased the rate and chemical yield of adduct **39c** [353 K: k_{obs} = 1.89(3) × 10^{-4} s^{-1} (THF-d_8), 1.54(3) × 10^{-4} s^{-1} (C_6D_{12})]. Therefore, to obtain activation parameters of the reaction, kinetic data were collected with a small excess use of Et_3PO in THF-d_8 solvent (entries 5−9 in Table 9).

Activation parameters were estimated using the Eyring plot (see Figure S7 in the Supporting Information) to be $\Delta H^{\ddagger}$ = 28.5 ± 1.0 kcal mol^{-1}, $\Delta S^{\ddagger}$ = 6.1 ± 2.7 eu, and $\Delta G_{298}{}^{\ddagger}$ = 26.7 ± 1.8 kcal mol^{-1}. These values are quite comparable to those obtained in the reaction of **7** with naphthalene. The small value of $|\Delta S^{\ddagger}|$, as well as the reaction rates independent from [Et_3PO], clearly indicate that the rate-determining step is involved in the formation of σ-complex $\mathbf{II_{Ph}}$ from **7** (reductive coupling), which is an only nonassociative and nondissociative step in the proposed mechanism (Scheme 14).

4. Theoretical Consideration. DFT calculations at the B3LYP level were performed on the geometrical and electronic structures of $\mathbf{I_R}$ (R = Ph (**7**), Me (**10**), CH_2SiMe_3 (**12**), 2-naphthyl (**13b**), and its naphthyl ring rotamer (**13b′**)), $\mathbf{II_R}$ (R = Ph, Me, and 2-naphthyl), **III**, and **39b**. Although the naphthyl-ring rotamer **13b′** was slightly higher in energy than **13b** (see Table S3 and Figure S13 in the Supporting Information), the former was found to have more structural relation to the corresponding transition state. Therefore, the reaction profiles from **7** or **10** to **13b′** via the transition states $\mathbf{TS(I_R\text{-}II_R)}$ (R = Ph or Me and 2-naphthyl) and intermediates $\mathbf{II_R}$ (R = Ph or Me and 2-naphthyl) were calculated. As listed in Table 10, the structural parameters of the DFT-optimized **7**, **13b**, and **39b** were found to be in good accordance with those of their crystal structures except for the M−H, H−H, and Cp(cent)−Ir distances. Optimized structures of **II** share several structural features with those of optimized **39b** in terms of key atomic distances, Zr−Ir (2.50−2.52 Å vs 2.53 Å), Ir−H(av) (1.65 Å vs 1.64 Å), and H−H (2.27−2.29 Å vs 2.25 Å), and the three-legged piano stool geometries of each metal but differ from **39b** in the Ir ligand *endo*/*exo* conformation.

The common geometrical features of $\mathbf{II_R}$ (R = Ph, Me, and 2-naphthyl) and **39b**, and bonding orbital interactions between Zr and Ir atoms in these species were explored. MO131 and MO138 for $\mathbf{II_{Ph}}$ and MO141 and MO149 for **39b** are shown in Figure 9 (MO114 and MO122 for $\mathbf{II_{Me}}$ in Figure S14 in the Supporting Information and MO143 and MO151 for $\mathbf{II_{Naph}}$ in Figure S15 in the Supporting Information). The Zr−Ir σ-bonding interaction is explicitly observed in HOMO-8 for $\mathbf{II_{Ph}}$ and **39b** while their HOMOs display large but incomplete Zr(d_π)−Ir(d_π) orbital overlaps and two antibonding orbital interactions between Ir and three cyclopentadienyl-ring carbons. In each complex, the two intermetal bonding interactions might not exclude a possibility of Zr−Ir double bonding. Similarly, Zr−Ir bonding and antibonding molecular orbitals for optimized **III** are shown in Figure 10. The two bonding orbital interactions of HOMO and HOMO-8 are comparable to those of $\mathbf{II_{Ph}}$, $\mathbf{II_{Me}}$, $\mathbf{II_{Naph}}$, and **39b**. The LUMO of **III** displays Zr-based d_{z2} orbital, probably reflecting its Lewis acid character. These orbital interactions of **III** are quite similar to those of the reported {$Cp^*Ta(CH_2SiMe_3)_2$}(Cp^*IrH_2).[11]

As listed in Table 11, NBO analysis revealed that the Zr−Ir interaction involves at least a single covalent bond [Wiberg bond index = 1.064−1.103 (**II**), 1.156 (**III**), and 1.021 (**39b**)] while much smaller values were observed in **I** [Zr−Ir: Wiberg bond index = 0.364−0.378].[47] Also, the Cp^*IrH_2 fragment in each structure proved to have more ionic character in comparison to that in {$Cp^*Ta(CH_2SiMe_3)_2$}(Cp^*IrH_2)[11] and (Cp^*Ir)(μ-H)$_3$ fragment of **I** [NBO total charge for Cp^*IrH_2 fragment: −0.520 to −0.559 (**II**), −0.574 (**III**), −0.697 (**39b**), and −0.254 ({$Cp^*Ta(CH_2SiMe_3)_2$}(Cp^*IrH_2)); NBO total charge for (Cp^*Ir)(μ-H)$_3$ fragment: −0.166 to −0.192 (**I**)], although the Zr−Ir covalent bond connecting the two fragments is thought to be intrinsically polarized. In other words, the presence of a secondary ionic interaction, in addition to the covalent σ-bond between Zr and Ir, could be considered for the Zr−Ir bonding structure of **II**, **III**, and **39b** rather than covalent double bonds (see Chart 2). According to the calculation data (Table 11), the degree of the charged Zr−Ir single bond or covalent double bond in {$L^1Zr(L)$}(Cp^*IrH_2) (L = none, R−H, $OPEt_3$) seems to be dependent upon the nature of the ligand L on the Zr; The greater electron donation of L [charge of L: none < Me−H < Ph−H, Naph−H < $OPEt_3$] has a tendency to decrease the covalent bond index.

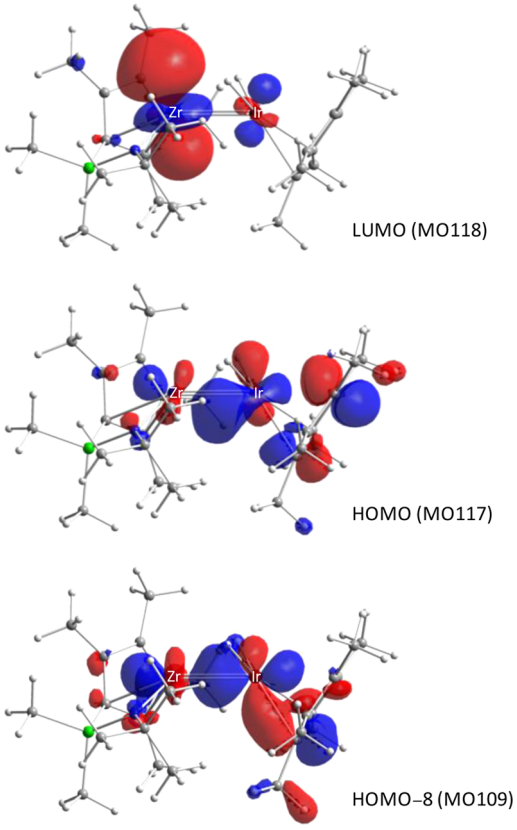

Figure 10. HOMO-8 (−6.89 eV), HOMO (−4.48 eV), and LUMO (−1.95 eV) of optimized **III**.

On the basis of the calculation for finding saddle point reaction diagrams for **7** → **13b′** and **10** → **13b′** are described in Figure 11 and Figure S16 in the Supporting Information, respectively. Although we have not been able to determine transition state structures for two reaction steps by the DFT method (**II** → **III** and **III** → **39b**), the existence of **III** as the common intermediate in the reaction diagrams is energetically feasible.[48]

The calculated $\Delta G_{298}{}^{\ddagger}$ values for **7** → $\mathbf{II_{Ph}}$ (23.5 kcal mol^{-1}) and **10** → $\mathbf{II_{Me}}$ (26.1 kcal mol^{-1}) have good agreement with the

dx.doi.org/10.1021/ic500258g | Inorg. Chem. 2014, 53, 6634−6654

Table 11. Wiberg Index and Natural Charge of Optimized Complexes I_R, II_R, III, and 39b (NBO Basis)

complex	7	10	12	13b	13b′	II_{Ph}	II_{Me}	II_{Naph}	III	39b
				Wiberg Index						
Zr−Ir	0.378	0.364	0.369	0.377	0.375	1.064	1.103	1.065	1.156	1.021
Zr−N	0.771	0.746	0.744	0.769	0.773	0.761	0.754	0.747	0.699	0.654
Zr−H	0.216	0.212	0.213	0.213	0.215	0.233	0.222	0.230	0.209	0.216
	0.241	0.235	0.237	0.243	0.240	0.283	0.273	0.279	0.258	0.232
	0.215	0.218	0.218	0.215	0.214					
Ir−H	0.530	0.539	0.535	0.533	0.530	0.550	0.564	0.553	0.572	0.571
	0.514	0.519	0.517	0.512	0.515	0.516	0.521	0.520	0.527	0.554
	0.536	0.537	0.534	0.535	0.537					
Zr−C_R or Zr−O	0.622	0.706	0.650	0.619	0.618	0.111	0.104	0.113		0.333
C_R−H or P−O						0.858	0.884	0.864		0.936
				Natural Charge						
Zr	1.443	1.471	1.485	1.445	1.447	1.291	1.309	1.308	1.492	1.471
Ir	0.152	0.144	0.142	0.144	0.144	−0.072	−0.067	−0.083	−0.082	−0.145
N	−1.273	−1.284	−1.282	−1.274	−1.274	−1.273	−1.285	−1.282	−1.313	−1.315
H	−0.066	−0.053	−0.067	−0.064	−0.067	−0.080	−0.070	−0.078	−0.085	−0.094
	−0.076	−0.080	−0.064	−0.077	−0.076	−0.100	−0.101	−0.100	−0.122	−0.108
	−0.039	−0.058	−0.055	−0.035	−0.037					
C_R or O	−0.453	−1.139	−1.434	−0.445	−0.445	−0.305	−0.874	−0.302		−1.133
(Cp*Ir)(μ-H)$_3$ or Cp*IrH$_2$	−0.166	−0.192	−0.176	−0.167	−0.172	−0.541	−0.520	−0.559	−0.574	−0.697
R−H or $OPEt_3$						0.082	0.064	0.085	0	0.186

Chart 2. Two Possible Structural Extremes of Zr−Ir Bonding in II_R

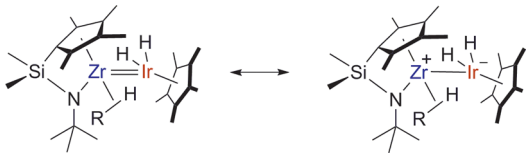

experimental values [7 → **13b**: 26.6(8) kcal mol^{-1}; **10** → **13b**: 26.2(6) kcal mol^{-1}]. Calculations for the reaction of **7** to form $\mathbf{II_{Ph}}$ in cyclohexane solvent were also examined, resulting in negligible differences from the gas-phase calculations (see Table S3 in the Supporting Information). Since the free energy of the common species **III** in the reactions of **7** → **III** and **10** → **III** can be anchored, the free-energy difference at 298 K between $\mathbf{II_{Me}}$ + C_6H_6 and $\mathbf{II_{Ph}}$ + CH_4 is ∼1.18 kcal mol^{-1} (see Table S4 in the Supporting Information) (greater difference between $\mathbf{TS(10\text{-}II_{Me})}$ + C_6H_6 and $\mathbf{TS(7\text{-}II_{Ph})}$ + CH_4: 2.86 kcal mol^{-1}; see Table S5 in the Supporting Information), and may account for the slightly disfavored ligand exchange of **7** → **10**.

V. Attempted Transmetalation. Zirconocene-catalyzed hydro- and carbo-aluminations provide stereoselective preparation of carbon nucleophiles from alkenes and alkynes.[49,50] In contrast to these ubiquitous unsaturated substrates, utility of aromatic hydrocarbons has been much less developed for the key transmetalation using aluminum reagents.[51] Since we developed incorporation of various aromatic substrates into the Zr−Ir complex via C−H activation, transmetalation from the Zr−Ir system to Al was thus investigated. In early works by Schwartz and co-workers on stoichiometric hydrozirconation of C−C unsaturations with $Cp_2Zr(H)Cl$ and subsequent transmetalation to aluminum reagents, they demonstrated that R_2AlCl (R = Cl, Me, ^{i}Bu) are the choice of reagents and the transmetalated products display higher synthetic values than the raw hydrozirconation intermediates.[52]

Reactions of **7** with Me_3Al and Me_2AlCl were thus tested in C_6D_{12} solvent and the reaction progress was traced by ^{1}H NMR spectroscopy. These reactions led to the formation of desirable transmetalated Me_2AlPh under the given conditions, accompanied by complexes **10** and **5** (Scheme 15).

The former reaction was rather sluggish, even with use of excess Me_3Al. In addition, increasing the reaction temperature caused a side reaction of the once-formed **10** with the remaining Me_3Al. The reaction of **10** and Me_3Al at 60 °C was carefully monitored by ^{1}H NMR analysis; after heating for 10 h, dihydrido complex (L^1ZrMe)(Cp*IrAlMe$_2$)(μ-H)$_2$ (**40**) was formed in high yield, with the evolution of methane (see Scheme 16). **40** was readily isolated as light yellow crystals and the structure was confirmed by spectroscopic, X-ray crystallographic, and combustion analyses. The Zr−Ir distance in the solid-state structure of **40** (2.6853(3) Å; see Figure 12) is significantly longer than that in the aforementioned dihydride **39**. The bond distances and angles of Ir in **40** suggest a

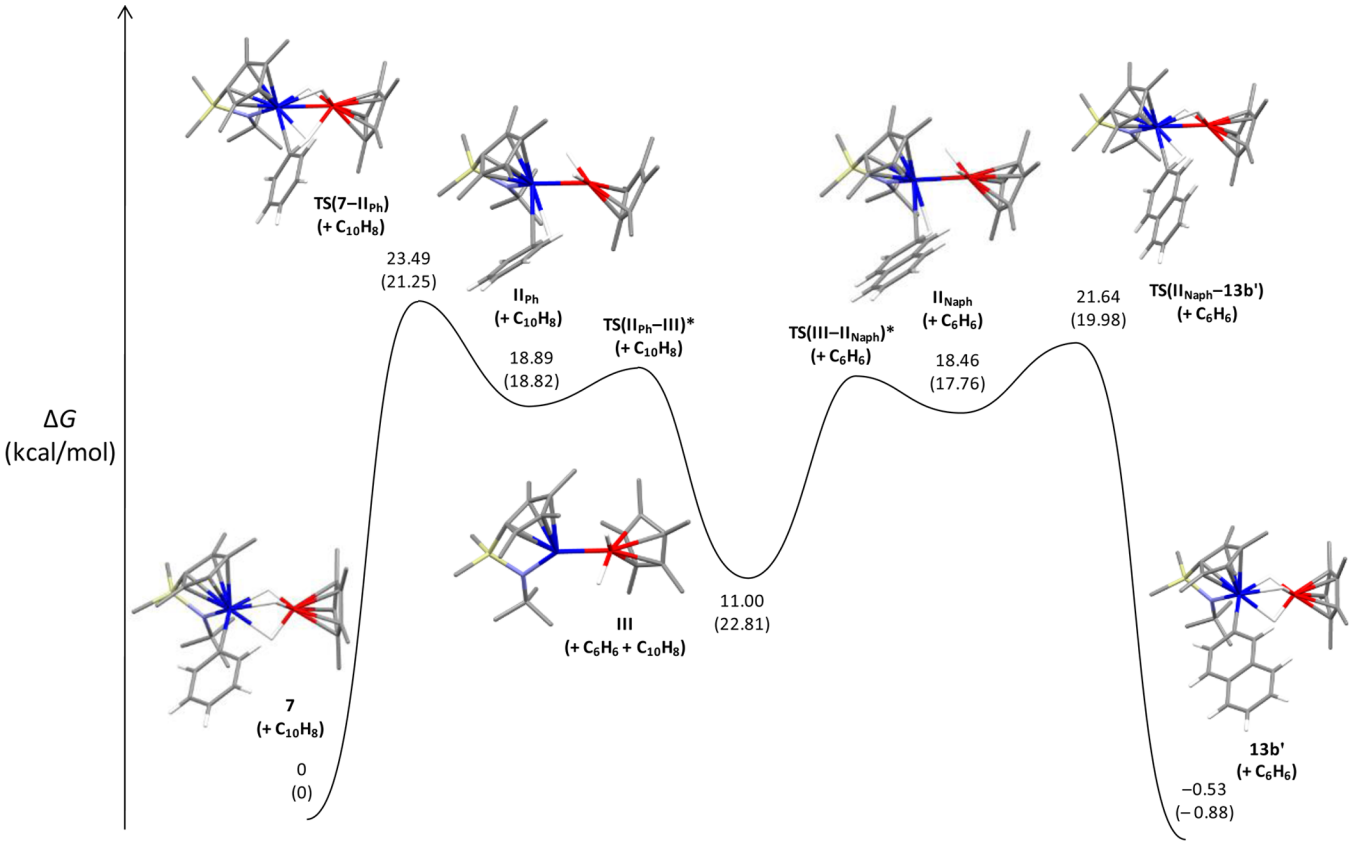

Figure 11. Reaction coordinates for the reaction of **7** to **13b′**. Values shown in parentheses indicate zero-point energies.

Scheme 15. Phenyl Group Transfer from 7 to Aluminum

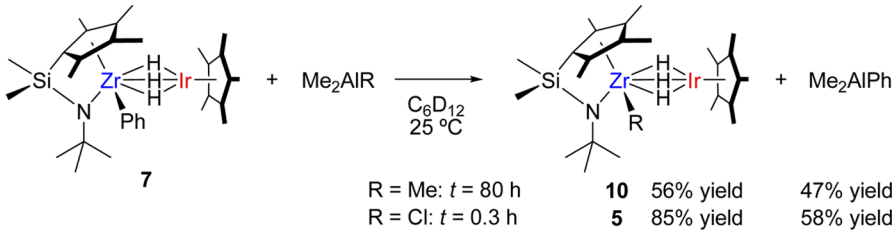

Scheme 16. Formation of 40

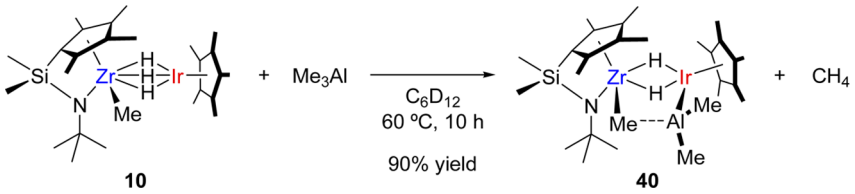

three-legged piano stool geometry of Cp*Ir with two non-equivalent bridging hydrides and covalently bonded Al [Ir–Al = 2.5134(1) Å, Ir–H(av) = 1.54 Å; Al–Ir–*H* = 84.9° and 89.1°; H–Ir–*H* = 94.3°].[53] Therefore, the structural features imply the absence of strong Zr–Ir bonding interaction.

Two mechanistic scenarios can be drawn for the formation of **40**. One is a concerted mechanism via four-centered σ-bond metathesis between Ir–H and Al–Me on the (Cp*Ir)(μ–H)$_3$ fragment only, and the other reductive elimination of methane from **10**, followed by oxidative addition of Al–Me bond into **III**. No (labeling) experiment to address the mechanism has been attempted, because ready scrambling between the Zr–Me bond in **10** and AlMe$_3$ can be expected. Because of the relative ease of methane elimination from **10**, in comparison to benzene elimination from **7** and steric repulsion between the Ir ligand set and Me$_3$Al, the latter reductive elimination/oxidative addition mechanism is thought to be more plausible. Apart from the analysis, thermal robustness of **40** did not allow reversible Me$_3$Al elimination from **40** in the presence of excess benzene that had been hoped to regenerate **7** or the key intermediate **III** to activate C–H bond of external arene substrates for a catalytic cycle.[54]

dx.doi.org/10.1021/ic500258g | Inorg. Chem. 2014, 53, 6634–6654

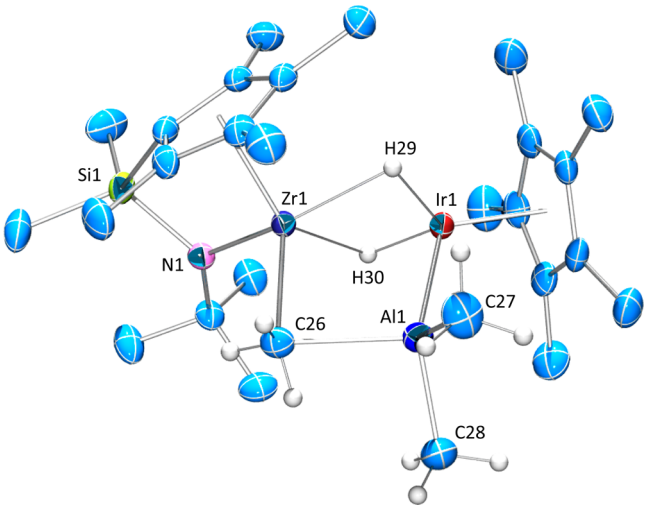

Figure 12. Molecular structure of **40**. Hydrogen atoms except for bridging hydrides and methyl protons on zirconium and aluminum are omitted for the sake of clarity. Selected bond lengths (Å) and angles (deg): Zr1−Ir1, 2.6853(3) Å; Zr1−N1, 2.104(2) Å; Zr1−C26, 2.375(3) Å; Ir1−Al1, 2.5133(9) Å; Ir1−H29, 1.57 Å; Ir1−H30, 1.50 Å; Al1−C26, 2.272(3) Å; Al1−C27, 1.981(3) Å; Al1−C28, 1.994(3) Å; Zr1−Cp(cent), 2.215 Å; and Ir1−Cp(cent), 1.893. Zr1−Ir1−Cp(cent), 170.42°; Ir1−Zr1−C26, 101.03(8)°; Zr1−Ir1−Al1, 69.63(2)°; H29−Ir1−H30, 94.3°; Al1−Ir1−H29, 84.6°; Al1−Ir1−H30, 89.1°; Ir1−Zr1−Cp(cent) 124.65°; and N1−Zr1−Cp(cent), 101.70°.

■ CONCLUSIONS

Dinuclear Zr−Ir hydrides $(L^1ZrR)(Cp^*Ir)(\mu\text{-}H)_3$ were designed and synthesized to investigate the C−H bond activation of aromatic and organometallic compounds under thermolytic conditions. The regioselective C−H bond cleavage of pyridine and methoxyarene substrates with complex **7** was observed, suggesting the formation of a Lewis acidic active intermediate (**III**), which could undergo precoordination at the Zr center with the heteroatoms and successive oxidative addition of the *ortho* C−H bond in these substrates. The trapping of **III** with Lewis basic reagents was then undertaken. The isolation and characterization of the corresponding Et_3PO-adduct of **III** (**39b**) was successfully achieved. This outcome proved that the unsupported Zr−Ir bond of **39b** was formed from the starting complex **7**, which did not have strong Zr−Ir interactions (>7% contraction, compared to that in **7**). The kinetic studies of the ligand exchange using either **7** or **10** with excess naphthalene and the formation of **39b** clearly revealed that these reactions proceeded through the σ-complexes of **III** ($\mathbf{II_{Ph}}$ or $\mathbf{II_{Me}}$) as the transient intermediates. In addition, the experimental observations were supported by the results of the DFT calculations. Moreover, the results of the NBO analysis suggested that the bonding structures in the intermediates (**II** and **III**) and adduct (**39b**) were commonly composed of both covalent and ionic bonds (multiple bonding interactions). This was reminiscent of the more covalent Ta−Ir bonding observed in our recent work.[11] Our analysis underscored the fact that strong and reactive bonding phenomena between early and late transition elements could occur in such molecular systems as well.

■ ASSOCIATED CONTENT

Supporting Information

Experimental procedures and characterization of new complexes, computational details, and X-ray data for L^1ZrPh_2, L^1ZrBr_2, **5**−**7**, *syn*-**9**, *anti*-**9**, **12**, **13b**, **15a**, **17**, **18**, **20**, **22**, **23**, **26**, **27**, **31**, **33**−**36**, **38**, **39b**, and **40** (PDF and CIF files). This material is available free of charge via the Internet at http://pubs.acs.org.

■ AUTHOR INFORMATION

Corresponding Author

*E-mail: hiroharu@o.cc.titech.ac.jp.

Notes

The authors declare no competing financial interest.

■ ACKNOWLEDGMENTS

We thank the Japan Society for the Promotion of Science for supporting this research through a Grant-in-Aid for Scientific Research (S) (Grant No. 18105002).

■ REFERENCES

(1) (a) Morales, F.; Weckhuysen, B. M. *Catalysis* **2006**, *19*, 1. (b) Khodakov, A. Y.; Chu, W.; Fongarland, P. *Chem. Rev.* **2007**, *107*, 1692.

(2) (a) Tauster, S. J.; Fung, S. C.; Baker, R. T. K.; Horsley, J. A. *Science* **1981**, *211*, 1121. (b) Tauster, S. J. *Acc. Chem. Res.* **1987**, *20*, 390.

(3) (a) Casey, C. P.; Bullock, R. M.; Nief, F. *J. Am. Chem. Soc.* **1983**, *105*, 7574. (b) Bullock, R. M.; Casey, C. P. *Acc. Chem. Res.* **1987**, *20*, 167. (c) Casey, C. P.; Palermo, R. E.; Jordan, R. F.; Rheingold, A. L. *J. Am. Chem. Soc.* **1985**, *107*, 4597. (d) Casey, C. P.; Palermo, R. E.; Rheingold, A. L. *J. Am. Chem. Soc.* **1986**, *108*, 549.

(4) (a) Stephan, D. W. *Coord. Chem. Rev.* **1989**, *95*, 41. (b) Hey-Hawkins, E. *Chem. Rev.* **1994**, *94*, 1661. (c) Wheatley, N.; Kalck, P. *Chem. Rev.* **1999**, *99*, 3379. (d) Gade, L. H. *Angew. Chem., Int. Ed.* **2000**, *39*, 2658. (e) Ritleng, V.; Chetcuti, M. J. *Chem. Rev.* **2007**, *107*, 797.

(5) Sartain, W. J.; Selegue, J. P. *J. Am. Chem. Soc.* **1985**, *107*, 5818.

(6) Gade, L. H.; Memmler, H.; Kauper, U.; Schneider, A.; Fabre, S.; Bezougli, I.; Lutz, M.; Galka, C. H.; Scowen, I. J.; McPartlin, M. *Chem.—Eur. J.* **2000**, *6*, 692.

(7) (a) Baranger, A. M.; Bergman, R. G. *J. Am. Chem. Soc.* **1994**, *116*, 3822. (b) Curley, J. J.; Bergman, R. G.; Tilley, T. D. *Dalton Trans.* **2012**, *41*, 192.

(8) (a) Bosch, B.; Brümmer, I.; Kunz, K.; Erker, G.; Fröhlich, R.; Kotila, S. *Organometallics* **2000**, *19*, 1255. (b) Cornelißen, C.; Erker, G.; Kehr, G.; Fröhlich, R. *Dalton Trans.* **2004**, 4059. (c) Cornelissen, C.; Erker, G.; Kehr, G.; Fröhlich, R. *Organometallics* **2005**, *24*, 214.

(9) Ferguson, G. S.; Wolczanski, P. T.; Párkányi, L.; Zonnevylle, M. C. *Organometallics* **1988**, *7*, 1967.

(10) (a) Greenwood, B. P.; Rowe, G. T.; Chen, C.-H.; Foxman, B. M.; Thomas, C. M. *J. Am. Chem. Soc.* **2010**, *132*, 44. (b) Setty, V. N.; Zhou, W.; Foxman, B. M.; Thomas, C. M. *Inorg. Chem.* **2011**, *50*, 4647. (c) Krogman, J. P.; Foxman, B. M.; Thomas, C. M. *J. Am. Chem. Soc.* **2011**, *133*, 14582.

(11) Oishi, M.; Kino, M.; Saso, M.; Oshima, M.; Suzuki, H. *Organometallics* **2012**, *31*, 4658.

(12) Oishi, M.; Suzuki, H. *Inorg. Chem.* **2009**, *48*, 2349.

(13) Reviews; see: (a) Arndtsen, B. A.; Bergman, R. G.; Mobley, T. A.; Peterson, T. H. *Acc. Chem. Res.* **1995**, *28*, 154. (b) Jones, W. D.; Feher, F. J. *Acc. Chem. Res.* **1989**, *22*, 91. (c) Jones, W. D. In *Topics in Organometallic Chemistry*; Murai, S., Ed.; Springer−Verlag: New York, 1999; Vol. 3, p 9. (d) Crabtree, R. H. *J. Chem. Soc., Dalton Trans.* **2001**, 2437.

(14) Group 4 metal complexes; see: (a) Lee, H.; Desrosiers, P. J.; Guzei, I.; Rheingold, A. L.; Parkin, G. *J. Am. Chem. Soc.* **1998**, *120*, 3255. (b) Bernskoetter, W. H.; Pool, J. A.; Lobkovsky, E.; Chirik, P. J. *Organometallics* **2006**, *25*, 1092. (c) Walsh, P. J.; Hollander, F. J.; Bergman, R. G. *J. Am. Chem. Soc.* **1988**, *110*, 8730. (d) Cummins, C. C.; Baxter, S. M.; Wolczanski, P. T. *J. Am. Chem. Soc.* **1988**, *110*, 8731. (e) Schaller, C. P.; Cummins, C. C.; Wolczanski, P. T. *J. Am. Chem.*

Soc. **1996**, *118*, 591. (f) Bailey, B. C.; Fan, H.; Huffman, J. C.; Baik, M.-H.; Mindiola, D. J. *J. Am. Chem. Soc.* **2007**, *129*, 8781.

(15) Group 9 metal complexes; see: (a) Janowicz, A. H.; Bergman, R. G. *J. Am. Chem. Soc.* **1982**, *104*, 352. (b) Hoyano, J. K.; McMaster, A. D.; Graham, A. G. *J. Am. Chem. Soc.* **1982**, *104*, 3723. (c) Jones, W. D.; Feher, F. J. *J. Am. Chem. Soc.* **1982**, *104*, 4240. (d) Wong-Foy, A. G.; Bhalla, G.; Liu, X. Y.; Periana, R. A. *J. Am. Chem. Soc.* **2003**, *125*, 14292.

(16) Carpenetti, D. W.; Kloppenburg, L.; Kupec, J. T.; Petersen, J. L. *Organometallics* **1996**, *15*, 1572.

(17) (a) Cotton, F. A.; Murillo, L. A.; Walton, R. A. *Multiple Bonds Between Metal Atoms*, 3rd Edition; Springer: New York, 2005. (b) Pauling, L. *The Nature of the Chemical Bond*, 3rd Edition; Cornell University Press: Ithaca, NY, 1960.

(18) (a) Gilbert, T. M.; Hollander, F. J.; Bergman, R. G. *J. Am. Chem. Soc.* **1985**, *107*, 3508. (b) Lin, Z.; Hall, M. B. *Organometallics* **1992**, *11*, 3801.

(19) Oishi, M.; Kato, T.; Nakagawa, M.; Suzuki, H. *Organometallics* **2008**, *27*, 6046.

(20) (a) Jeffery, J.; Lappert, M. F.; Luong-Thi, N. T.; Atwood, J. L.; Hunter, W. *J. Chem. Soc., Chem. Commun.* **1978**, 1081. (b) Courtot, P.; Pichon, R.; Salaun, J. Y.; Toupet, L. *Can. J. Chem.* **1991**, *69*, 661. (c) Lee, H.; Bridgewater, B. M.; Parkin, G. *J. Chem. Soc., Dalton Trans.* **2000**, 4490.

(21) Ligand exchange of **10** with C_6D_6 at 50 °C (entry 3 in Table 3) was monitored by ^{1}H NMR spectroscopy. Unlike the reaction of **10** at 70 °C and the reaction of **11** at 25 °C (entries 4 and 5 in Table 3), $(L^1ZrC_6D_5)(Cp^*Ir)(\mu\text{-}H)_3$ was detected at the initial stage, implying temperature dependence of the exchange mechanism of **10**.

(22) (a) Schock, L. E.; Marks, T. J. *J. Am. Chem. Soc.* **1988**, *110*, 7701. (b) Simoes, J. A. M.; Beauchamp, J. L. *Chem. Rev.* **1990**, *90*, 629. (c) Siegbahn, P. E. M. *J. Phys. Chem.* **1995**, *99*, 12723.

(23) (a) Shilov, A. E.; Shul'pin, G. B. *Chem. Rev.* **1997**, *97*, 2879. (b) Bromberg, S. E.; Yang, H.; Asplund, M. C.; Lian, T.; McNamara, B. K.; Kotz, K. T.; Yeston, J. S.; Wilkens, M.; Frei, H.; Bergman, R. G.; Harris, C. B. *Science* **1997**, *278*, 260. (c) Labinger, J. A.; Bercaw, J. E. *Nature* **2002**, *417*, 507. (d) Crabtree, R. H. *J. Organomet. Chem.* **2004**, *689*, 4083. (e) Pérez, P. J. *Alkane C−H Activation by Single-Site Metal Catalysis*; Perez, P. J., Ed.; Catalysis by Metal Complexes, Vol. *38*; Springer: Dordrecht, The Netherlands, 2012.

(24) The bimetallic species seems to be stable in C_6D_6 solvent, even at 120 °C, but undergoes thermolytic C−H activation of the substrates, along with competitive decomposition in nonaromatic hydrocarbon solvents (e.g., C_6D_{12}), resulting in lower yields.

(25) Luo, Y.-R.; *Handbook of Bond Dissociation Energies in Organic Compounds*; CRC Press: Boca Raton, FL, 2002.

(26) Pd-catalyzed benzylic C−H borylation was proposed to undergo through a η^3-allyl intermediate. See: Ishiyama, T.; Ishida, K.; Takagi, J.; Miyaura, N. *Chem. Lett.* **2001**, 1082.

(27) (a) Ben-Ari, E.; Gandelman, M.; Rozenberg, H.; Shimon, L. J. W.; Milstein, D. *J. Am. Chem. Soc.* **2003**, *125*, 4714. (b) Ben-Ari, E.; Cohen, R.; Gandelman, M.; Shimon, L. J. W.; Martin, J. M. L.; Milstein, D. *Organometallics* **2006**, *25*, 3190. (c) Fan, L.; Parkin, S.; Ozerov, O. V. *J. Am. Chem. Soc.* **2005**, *127*, 16772. (d) Wu, H.; Hall, M. B. *J. Phys. Chem. A* **2009**, *113*, 11706.

(28) (a) Mkhalid, I. A. I.; Barnard, J. H.; Marder, T. B.; Murphy, J. M.; Hartwig, J. F. *Chem. Rev.* **2010**, *110*, 890. (b) Lyons, T. W.; Hull, K. L.; Sanford, M. S. *J. Am. Chem. Soc.* **2011**, *133*, 4455. (c) Zhang, F.; Kirby, C. W.; Hairsine, D. W.; Jennings, M. C.; Puddephatt, R. J. *J. Am. Chem. Soc.* **2005**, *127*, 14196. (d) Yanagisawa, S.; Sudo, T.; Noyori, R.; Itami, K. *J. Am. Chem. Soc.* **2006**, *128*, 11748.

(29) (a) Wittig, G.; Pockels, U. *Ber. Dtsch. Chem. Ges. B* **1939**, *72*, 89. (b) Fischer, R.; Gärtner, M.; Görls, H.; Yu, L.; Reiher, M.; Westerhausen, M. *Angew. Chem., Int. Ed.* **2007**, *46*, 1618. (c) Mulvey, R. E.; Mongin, F.; Uchiyama, M.; Matsumoto, Y. *Angew. Chem., Int. Ed.* **2007**, *46*, 3802. (d) Oyamada, J.; Nishiura, M.; Hou, Z. *Angew. Chem., Int. Ed.* **2011**, *50*, 10720.

(30) Arndt, P.; Lefeber, C.; Kempe, R.; Rosenthal, U. *Chem. Ber.* **1996**, *129*, 207.

(31) Wenkert, E.; Michelotti, E. L.; Swindell, C. S.; Tingoli, M. *J. Org. Chem.* **1984**, *49*, 4894.

(32) (a) Tanke, R. S.; Crabtree, R. H. *J. Am. Chem. Soc.* **1990**, *112*, 7984. (b) Crabtree, R. H. *New J. Chem.* **2003**, *27*, 771.

(33) Alkylation of pyridines by cationic zirconocenes: (a) Jordan, R. F.; Tayler, D. F. *J. Am. Chem. Soc.* **1989**, *111*, 778. (b) Jordan, R. F.; Taylor, D. F.; Baenziger, N. C. *Organometallics* **1990**, *9*, 1546. (c) Jordan, R. F.; Guram, A. S. *Organometallics* **1990**, *9*, 2116. (d) Guram, A. S.; Jordan, R. F. *Organometallics* **1990**, *9*, 2190. (e) Guram, A. S.; Jordan, R. F. *Organometallics* **1991**, *10*, 3470. (f) Guram, A. S.; Jordan, R. F.; Tayler, D. F. *J. Am. Chem. Soc.* **1991**, *113*, 1833. (g) Rodewald, S.; Jordan, R. F. *J. Am. Chem. Soc.* **1994**, *116*, 4491. (h) Dagorne, S.; Rodewald, S.; Jordan, R. F. *Organometallics* **1997**, *16*, 5541.

(34) Structurally well characterized η^2-pyridyl zirconocenes; see: (a) Bradley, C. A.; Lobkovsky, E.; Chirik, P. J. *J. Am. Chem. Soc.* **2003**, *125*, 8110. (b) Spannenberg, A.; Jäger-Fiedler, U.; Arndt, P.; Rosenthal, U. *Z. Krystallogr.* **2005**, *220*, 253. (c) Krut'ko, D. P.; Kirsanov, R. S.; Belov, S. A.; Borzov, M. V.; Churakov, A. V.; Howard, J. A. K. *Polyhedron* **2007**, *26*, 2864.

(35) Zr complexes with nonchelating thioether ligands; see: (a) Valloton, M.; Merbach, A. E. *Helv. Chim. Acta* **1975**, *58*, 2272. (b) Eshuis, J. J. W.; Tan, Y. Y.; Meetsma, A.; Teuben, J. H.; Renkema, J.; Evens, G. G. *Organometallics* **1992**, *11*, 362. (c) Gomes, P. T.; Green, M. L. H.; Martins, A. M. *J. Organomet. Chem.* **1998**, *551*, 133. (d) Hart, R.; Levason, W.; Patel, B.; Reid, G. *J. Chem. Soc., Dalton Trans.* **2002**, 3153. (e) Levason, W.; Patel, B.; Reid, G. *Inorg. Chim. Acta* **2004**, *357*, 2115. (f) Krut'ko, D. P.; Borzov, M. V.; Kirsanov, R. S.; Antipin, M. Y.; Churakov, A. V. *J. Organomet. Chem.* **2004**, *689*, 595.

(36) (a) Bradley, C. A.; Veiros, L. F.; Pun, D.; Lobkovsky, E.; Keresztes, I.; Chirik, P. J. *J. Am. Chem. Soc.* **2006**, *128*, 16600. (b) Bradley, C. A.; Veiros, L. F.; Chirik, P. J. *Organometallics* **2007**, *26*, 3191. (c) Liu, F.-C.; Yang, C.-C.; Chen, S.-C.; Lee, G.-H.; Peng, S.-M. *Dalton Trans.* **2007**, 3599.

(37) Ir alkyl hydrido complexes; see: (a) Gutiérrez-Puebla, E.; Monge, Á.; Nicasio, M. C.; Pérez, P. J.; Poveda, M. L.; Carmona, E. *Chem.—Eur. J.* **1998**, *4*, 2225. (b) Yuan, Y.; Jiménez, M. V.; Sola, E.; Lahoz, F. J.; Oro, L. A. *J. Am. Chem. Soc.* **2002**, *124*, 752. (c) Feller, M.; Karton, A.; Leitus, G.; Martin, J. M. L.; Milstein, D. *J. Am. Chem. Soc.* **2006**, *128*, 12400.

(38) (a) Wilkinson, G.; Guillard, R. D.; McCleverty, J. A. *Comprehensive Coordination Chemistry*, Vol. 3; Pergamon Press: Oxford, U.K., 1987. (b) Johnson, J. S.; Bergman, R. G. *J. Am. Chem. Soc.* **2001**, *123*, 2923. (c) Thorman, J. L.; Young, V. G., Jr.; Boyd, P. D. W.; Guzei, I. A.; Woo, L. K. *Inorg. Chem.* **2001**, *40*, 499.

(39) We have not been able to identify the common byproduct detected from the reactions of **7** and trialkylphosphine oxides. In the ^{1}H NMR spectrum, the structure possesses C_s-symmetry in a 1:2 ratio of Zr and $(Cp^*Ir)(\mu\text{-}H)_3$ fragments.

(40) Mayer, U.; Gutmann, V.; Gerger, W. *Monatsh. Chem.* **1975**, *106*, 1235.

(41) Beckett, M. A.; Brassington, D. S.; Coles, S. J.; Hursthouse, M. B. *Inorg. Chem. Commun.* **2000**, *3*, 530.

(42) Reported P−O bond lengths in R_3PO: R = Et [1.511(7) Å], Pr [1.495(5) Å], *c*-Hex [1.490(2) Å], CH_2CH_2CN [1.498(3) Å]. See: (a) Engelhardt, L. M.; Raston, C. L.; Whitaker, C. R.; White, A. H. *Aust. J. Chem.* **1986**, *39*, 2151. (b) Cotton, F. A.; Kibala, P. A.; Miertschin, C. S. *Inorg. Chem.* **1991**, *30*, 548. (c) Simons, R. S.; Sanow, L. M.; Galat, K. J.; Tessier, C. A.; Youngs, W. J. *Organometallics* **2000**, *19*, 3994. (d) Davies, J. A.; Dutremez, S.; Pinkerton, A. A. *Inorg. Chem.* **1991**, *30*, 2380. (e) Cotton, F. A.; Darensbourg, D. J.; Fredrich, M. F.; Ilsley, W. H.; Troup, J. M. *Inorg. Chem.* **1981**, *20*, 1869.

(43) Reviews: (a) Jones, W. D. *Acc. Chem. Res.* **2003**, *36*, 140. (b) Gómez-Gallego, M.; Sierra, M. A. *Chem. Rev.* **2011**, *111*, 4857.

(44) Group 6 and 7 metal complexes; see: (a) Bullock, R. M.; Headford, C. E. L.; Kegley, S. E.; Norton, J. R. *J. Am. Chem. Soc.* **1985**, *107*, 727. (b) Bullock, R. M.; Headford, C. E. L.; Hennessy, K. M.; Kegley, S. E.; Norton, J. R. *J. Am. Chem. Soc.* **1989**, *111*, 3897.

(c) Parkin, G.; Bercaw, J. E. *Organometallics* **1989**, *8*, 1172. (d) Churchill, D. G.; Janak, K. E.; Wittenberg, J. S.; Parkin, G. *J. Am. Chem. Soc.* **2003**, *125*, 1403. (e) Labella, L.; Chernega, A.; Green, M. L. H. *J. Chem. Soc., Dalton Trans.* **1995**, 395. (f) Green, J. C.; Jardine, C. N. *J. Chem. Soc., Dalton Trans.* **1998**, 1057. (g) Conway, S. L. J.; Dijkstra, T.; Doerrer, L. H.; Green, J. C.; Green, M. L. H. *J. Chem. Soc., Dalton Trans.* **1998**, 2689. (h) Gould, G. L.; Heinekey, D. M. *J. Am. Chem. Soc.* **1989**, *111*, 5502.

(45) Group 9 metal complexes; see: (a) Jones, W. D.; Feher, F. J. *J. Am. Chem. Soc.* **1985**, *107*, 620. (b) Jones, W. D.; Feher, F. J. *J. Am. Chem. Soc.* **1985**, *107*, 1650. (c) Jones, W. D.; Feher, F. J. *J. Am. Chem. Soc.* **1986**, *108*, 4814. (d) Buchanan, J. M.; Stryker, J. M.; Bergman, R. G. *J. Am. Chem. Soc.* **1986**, *108*, 1537. (e) Periana, R. A.; Bergman, R. G. *J. Am. Chem. Soc.* **1986**, *108*, 7332.

(46) Three-trial experiments and experiments with varied $[7]_0$ for the reaction at ca. 359 K showed identical results (see Table S1 in the Supporting Information).

(47) Bond orders between early and late transition-metal centers are often underestimated by DFT calculations, because of the significant contribution of electrostatic interactions and electron delocalizations. (See refs 4c and 4d.) Hence, the bond order of Zr−Ir in **II**, **III**, and **39b** (>1) can imply the presence of the strong covalency between single and double bonds.

(48) In Figure 11 and Figure S15 in the Supporting Information, we located the ΔG value of the unknown transition states **TS(II−III)** at a lower level of energy than those of **TS(I−II)** because, upon going from **II** to **III**, the energy was increased linearly, and the experimental results ruled out that the dissociative step **II→III** is the rate-determining one in the ligand elimination process.

(49) (a) Van Horn, D. E.; Negishi, E. *J. Am. Chem. Soc.* **1978**, *100*, 2252. (b) Negishi, E.; Yoshida, T. *Tetrahedron Lett.* **1980**, *21*, 1501. (d) Negishi, E.; Van Horn, D. E.; Yoshida, T. *J. Am. Chem. Soc.* **1985**, *107*, 6639. (e) Kondakov, D. Y.; Negishi, E. *J. Am. Chem. Soc.* **1996**, *118*, 1577.

(50) Reviews; see: (a) Negishi, E. *Acc. Chem. Res.* **1987**, *20*, 65. (b) Eisch, J. J. In *Comprehensive Organometallic Chemistry II*; Abel, E. A., Stone, F. G. A., Wilkinson, G., Eds.; Pergamon Press: Oxford, U.K., 1995; Vol. *11*, Chapter 6. (c) Negishi, E.; Tan, Z. *Diastereoselective, Enantioselective, and Regioselective Carboalumination Reactions Catalyzed by Zirconocene Derivatives*, In *Metallocenes in Regio- and Stereoselective Synthesis*; Takahashi, T., Ed.; Topics in Organometallic Chemistry, Vol. *8*; Springer: Berlin, 2005; p 139. (d) Parfenova, L. V.; Khalilov, L. M.; Dzhemilev, U. M. *Russ. Chem. Rev.* **2012**, *81*, 524.

(51) (a) Mole, T.; Jeffery, E. A. *Organoaluminum Compounds*; Elsevier: Amsterdam, 1972. (b) Eisch, J. J. In *Comprehensive Organometallic Chemistry II*; Abel, E. A., Stone, F. G. A., Wilkinson, G., Eds.; Pergamon Press: Oxford, U.K., 1995; Vol. *1*, Chapter 10. (c) Oishi, M. *Sci. Synth.* **2004**, *7*, 261.

(52) (a) Carr, D. B.; Schwartz, J. *J. Am. Chem. Soc.* **1977**, *99*, 638. (b) Shoer, L. I.; Gell, K.; Schwartz, J. *J. Organomet. Chem.* **1977**, *136*, C19. (c) Carr, D. B.; Schwartz, J. *J. Am. Chem. Soc.* **1979**, *101*, 3521.

(53) Covalently Ir−Al bonded complexes; see: (a) Fryzuk, M. D.; Huang, Li.; McManus, N. T.; Paglia, P.; Rettig, S. J.; White, G. S. *Organometallics* **1992**, *11*, 2979. (b) Golden, J. T.; Peterson, T. H.; Holland, P. L.; Bergman, R. G.; Andersen, R. A. *J. Am. Chem. Soc.* **1998**, *120*, 223.

(54) Cp_2NbH_3-catalyzed alumination of benzene C−H bond has been proposed as the first catalytic C−H functionalization using metal hydrido complexes. See: Parshall, G. W. *Acc. Chem. Res.* **1975**, *8*, 113.